A Numerical Model for the Interaction of Io-Generated Alfvén Waves with Jupiter's Magnetosphere and Ionosphere

Robert Louis Lysak[1], Ali H. Sulaiman[2], Fran Bagenal[3], and Frank J. Crary[3]

[1]Univerity of Minnesota
[2]University of Minnesota
[3]University of Colorado Boulder

December 7, 2022

Abstract

The interaction of Io with the co-rotating magnetosphere of Jupiter is known to produce Alfven wings that couple the moon to Jupiter's ionosphere. We present first results from a new numerical model to describe the propagation of these Alfven waves in this system. The model is cast in magnetic dipole coordinates and includes a dense plasma torus that is centered around the centrifugal equator. Results are presented for two density models, showing the dependence of the interaction on the magnetospheric density. Model results are presented for the case when Io is near the centrifugal and magnetic equators as well as when Io is at its northernmost magnetic latitude. The effect of the conductance of Jupiter's ionosphere is considered, showing that a long auroral footprint tail is favored by high Pedersen conductance in the ionosphere. The current patterns in these cases show a U-shaped footprint due to the generation of field-aligned current on the Jupiter-facing and Jupiter-opposed sides of Io, which may be related to the structure in the auroral footprint seen in the infrared by Juno. A model for the development of parallel electric fields is introduced, indicating that the main auroral footprints of Io can generate parallel potentials of up to 100 kV.

A Numerical Model for the Interaction of Io-Generated Alfvén Waves with Jupiter's Magnetosphere and Ionosphere

R. L. Lysak[1], A. H. Sulaiman[1], F. Bagenal[2], F. Crary[2]

[1]School of Physics and Astronomy, Minnesota Institute for Astrophysics, University of Minnesota, Minneapolis, MN;[2]Laboratory for Astrophysics and Space Physics, University of Colorado, Boulder, CO

Corresponding author: Robert L. Lysak (lysak001@umn.edu)

Key Points:

- The spacing of the main auroral spots in Io's footprint tail depends on the density profile assumed as well as the magnetic latitude of Io.
- Partial reflections at the boundary of the Io plasma torus lead to secondary reflections and weaker auroral spots between the main spots.
- The length of the auroral tail depends on the ionospheric conductance at Jupiter, with higher conductances leading to longer tails.

Abstract

The interaction of Io with the co-rotating magnetosphere of Jupiter is known to produce Alfvén wings that couple the moon to Jupiter's ionosphere. We present first results from a new numerical model to describe the propagation of these Alfvén waves in this system. The model is cast in magnetic dipole coordinates

and includes a dense plasma torus that is centered around the centrifugal equator. Results are presented for two density models, showing the dependence of the interaction on the magnetospheric density. Model results are presented for the case when Io is near the centrifugal and magnetic equators as well as when Io is at its northernmost magnetic latitude. The effect of the conductance of Jupiter's ionosphere is considered, showing that a long auroral footprint tail is favored by high Pedersen conductance in the ionosphere. The current patterns in these cases show a U-shaped footprint due to the generation of field-aligned current on the Jupiter-facing and Jupiter-opposed sides of Io, which may be related to the structure in the auroral footprint seen in the infrared by Juno. A model for the development of parallel electric fields is introduced, indicating that the main auroral footprints of Io can generate parallel potentials of up to 100 kV.

Plain Language Summary

Jupiter's moon Io generated electrical currents when it passes through Jupiter's magnetic field. These currents take the form of fluctuations in the magnetic field lines, much like the waves on a stringed musical instrument. Due to the motion of Io, these waves follow behind Io and bounce back and forth between Jupiter and the dense ionized gas emitted by Io. This process creates auroral emissions that can be observed, for example, with the Hubble Space Telescope.

1 Introduction

Alfvén waves have long been associated with the coupling of the moon Io with the ionosphere of Jupiter since the discovery by Bigg (1964) that the Jovian decametric radio emissions were modulated by the phase of Io in its orbit. Goldreich and Lynden-Bell (1969) identified Io as the generator of field-aligned current due to its motion relative to the co-rotating plasma at Jupiter. Goertz (1980) and Neubauer (1980) noted that this is due to the launching of Alfvén "wings" from the moving satellite. These Alfvén waves were identified by the Voyager 1 flyby of Jupiter (Acuña et al., 1981; Belcher et al., 1981). The reflection of these Alfvén waves from Jupiter's ionosphere was invoked by Gurnett and Goertz (1981) to explain the multiplicity of decametric radio emissions. The role of the plasma torus produced by the volcanic activity on Io at modifying the propagation of Alfvén waves was recognized by Bagenal (1983), who considered the reflecting Alfvén wave model in the context of plasma measurements from the Voyager mission. She noted that the travel time for Alfvén waves to propagate from Io to Jupiter depended on Io's position with respect to the plasma torus, which peaks at the centrifugal equator (i.e., the loci of points on each field line that is farthest from the rotation axis of Jupiter) at a angle of 7° from Io's orbital plane. The auroral emissions from Io were observed from the Infrared Telescope Facility (Connerney et al., 1993) and the Hubble Space Telescope (Bonfond et al., 2008, 2009; Clarke et al., 1996, 2002). The pre-Juno understanding of the Io-plasma interaction was summarized by Saur et al. (2004) and Bagenal and Dols (2020).

With the arrival of the Juno satellite at Jupiter in July, 2016, detailed measurements of particles and waves in Jupiter's magnetosphere became possible. In particular, the Juno orbit has made a number of high-latitude crossings of field lines magnetically connected to Io, indicating the presence of accelerated electrons and ions (Szalay et al., 2018, 2020) and Alfvén waves with a power law spectrum extending up to the proton gyrofrequency (Gershman et al., 2019; Sulaiman et al., 2020). Observations of the Io footprint tail have been made by the Jovian Infrared Auroral Mapper (JIRAM) instrument on Juno (Moirano et al., 2021; Mura et al., 2017, 2018), which indicate that the footprint tail is made up from a series of spots that at times appear to alternate positions with respect to the footprint of Io's orbit. The purpose of the present work is to show the first results from a numerical model of the Io interaction with Jupiter's magnetosphere and ionosphere to help understand this interaction.

The propagation of these Alfvén waves was considered qualitatively by Crary and Bagenal (1997) as well as Bonfond et al. (2008). More recently, Hinton et al. (2019) used a diffusive equilibrium model of the plasma density to construct ray paths for the reflecting Alfvén waves. On the other hand, Crary and Bagenal (1997) and Jacobsen et al. (2007) assumed a sharp gradient and straight magnetic field lines. A new model for the interaction of Io was introduced by Schlegel and Saur (2022) who used a Hall-MHD model to describe the interaction. They included the Hall conductivity in Io's ionosphere in an attempt to understand the

alternating auroral spots observed by Mura et al. (2018) and Moirano et al. (2021). However, this model apparently assumed perfect conductivity in the Jovian ionosphere and straight magnetic field lines.

In order to improve upon these earlier efforts, we have developed a model for the propagation of Alfvén waves from Io that is cast in a more realistic dipole geometry. We note that the orbit of Io is roughly in the equatorial plane of Jupiter, while the magnetic dipole moment is displaced by 10.25°, consistent with the dipole term in the spherical harmonic analysis of JRM33 (Connerney et al., 2022). (It should be noted that this tilt is 9.52° for the VIP4 model (Connerney et al., 1998) and 10.31° for the JRM09 model (Connerney et al., 2018); however, the results presented here are not too sensitive to the magnetic field model used.) The Io plasma torus is centered on the centrifugal equator, which is two-thirds of the distance from the rotational equatorial plane to the magnetic equatorial plane (e.g., Bagenal, 1983). Io is modeled as a cloud of Pedersen conductivity that is moving with respect to the co-rotating plasma of Jupiter's magnetosphere. Jupiter's ionospheres are modeled by a height-integrated Pedersen conductance. In this work, we will focus on the effects of the plasma distribution along the Io flux tube as well as the effect of different conductances on the field-aligned current signatures from Io. The next section will describe the model, followed by a discussion of the effect of the density profile. The following section will consider variations in the conductance of Jupiter's ionosphere. Then the effect of parallel electric fields due to kinetic effects will be considered. We will conclude with a discussion of the implications of these results for the structure of the auroral footprint tail of Io.

2 Model Description

The model presented here is the latest version of a series of models to describe the propagation of Alfvén waves in magnetospheric geometries. Previous versions of this model have been used in the magnetosphere of Earth, where it has been used to describe the structure of field line resonances and cavity modes in response to the propagation of Pi2 pulsations (Lysak et al., 2015; Takahashi et al., 2022), interplanetary shock impacts (Takahashi et al., 2018) and the excitation of quarter-wave modes due to interhemispheric asymmetry in the ionosphere (Lysak et al., 2020). Versions of this model have also been used to study field line resonances at Jupiter (Lysak & Song, 2020) and the effect of the ionospheric Alfvén resonator at Jupiter (Lysak et al., 2021). The model is cast into magnetic dipolar coordinates, defined in terms of magnetic spherical coordinates by

Here ν is the negative inverse of the L-shell parameter and points outwards (we will use L-shell in this paper rather than the M-shell used when non-dipolar fields are important to indicate that we are using a dipolar geometry, which is a reasonable approximation at the orbit of Io), φ is the magnetic east longitude, defined so that it corresponds with System III Right-Handed coordinates at the points where Juno crosses the magnetic equator, and μ is a field-aligned coordinate, proportional to the magnetic scalar potential of the dipole field. This coordinate increases from south to north, opposite the direction of the Jovian magnetic field. Note that we will use east longitudes throughout this paper, although west longitudes are often used by Earth-based observers since the west longitude increases with time as seen from Earth as Jupiter rotates. For simplicity, we consider only the shear Alfvén mode; however, we can include the effect of parallel electric fields due to electron inertia or kinetic effects. In this case the relevant electrodynamic equations are

Here we have introduced the scale factors , and , where$R_J = 71492$ km is the equatorial radius of Jupiter, $B_J = 417.7$ μT is the equatorial dipole magnetic field at the surface of Jupiter according to JRM33 (this value is 426.4 μT for the VIP4 model and 419.9 μT for JRM09). We use where is the non-relativistic Alfvén speed to denote the Alfvén speed including the displacement current. The coefficient ν* is a parameter to characterize the kinetic effects (such as the development of double layers) that can lead to parallel electric fields in strong current regions. This parameter will be set to zero until the last section of this manuscript.

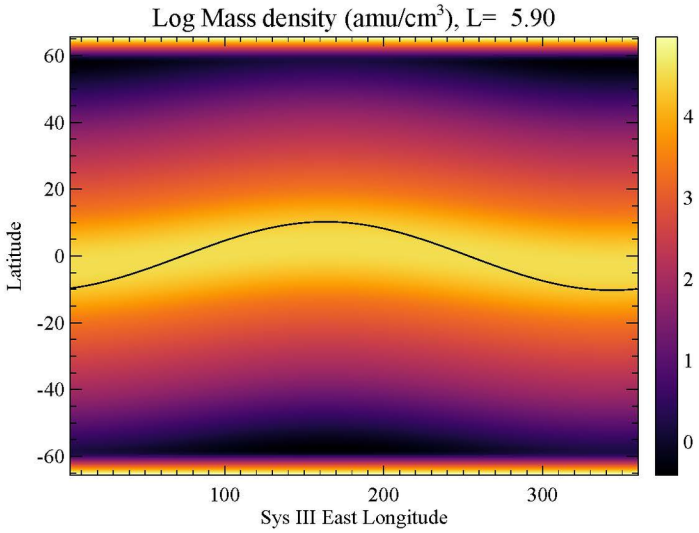

The equations are modeled in a frame co-rotating with Jupiter's magnetosphere. In this frame, Io moves westward at a speed of 57 km/s, leading to an emf of $V_{Io}B_0$ of 120 mV/m. This effect is included in the second term in the equation for E_ν in equation . Io is modeled as a cloud of conductivity which is constant over the diameter of Io and falls off as the distance squared in Io's ionosphere. As noted above, the simulation is based on magnetic coordinates, so that Io moves in a plane inclined about 10° from the magnetic equator. Similarly, the mass density in the Io plasma torus is centered on the centrifugal equator. We use two density profiles: a "high-density" case based on the density model of Dougherty et al. (2017), and a "low-density" case based on the model considered by Ray et al. (2009). These densities are taken to be independent of longitude along the centrifugal equator. The density and the resulting Alfvén speed c_A are plotted in Figure 1, with Figures 1a and 1b giving the density for the low- and high-density cases, respectively, while Figures 1c and 1d show the corresponding Alfvén speed profiles. The high-density case results in a density of 200 cm^{-3} at a radial distance of 2 R_J, while the low-density case has 0.1 cm^{-3} at this altitude. The trajectory of Io in magnetic coordinates is plotted as a solid line in these figures. These models have a total Alfven transit time from one ionosphere to the other of 16 minutes in the high-density case and 12 minutes in the low-density case. These values are comparable to the one-way transit times between 12.5 and 15 minutes in the model of Hinton et al. (2019).

3 Results: Effects of density model and longitude

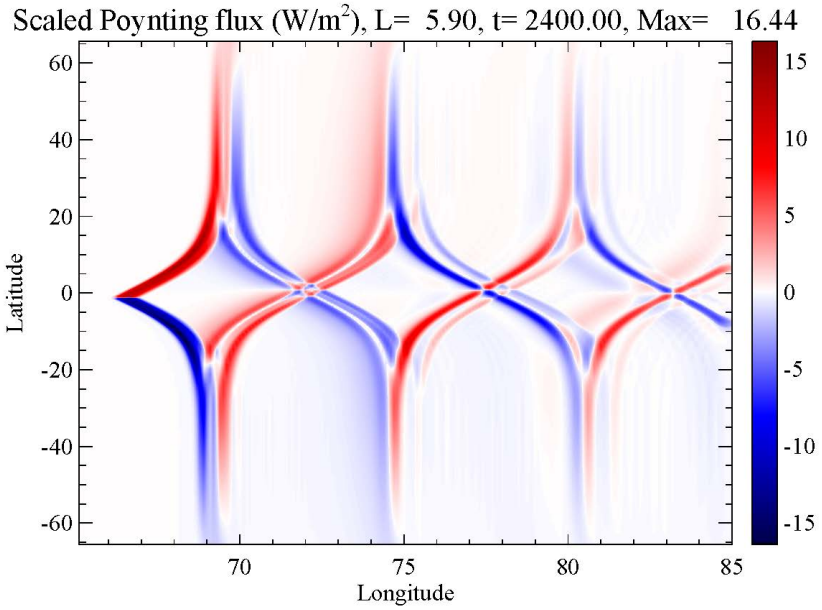

With this numerical model, we can simulate the propagation of Alfvén waves from Io at various points along Io's orbit. First, consider a case where Io is near the centrifugal equator, so that the Alfvén travel times from Io to each hemisphere are approximately the same. The Pedersen conductance of both ionospheres is set at 1 mho for these runs. Figure 2 shows the parallel component of the wave Poynting flux for such a case, 40 minutes from the start of the run. Io starts at 85° longitude (at the right side of the figure) and propagates westward. Note that Io crosses the centrifugal and magnetic equators at 74.3°. In this figure, red colors indicate northward Poynting flux while blue colors indicate southward flux, with the intensity of the colors indicating the magnitude. The magnitude of the Poynting flux is scaled by the background magnetic field to account for the smaller flux tube radius as the wave approaches each ionosphere. Figure 2a shows the results from the low-density case, while the high-density case is given in Figure 2b. As expected, the northern and southern wave patterns are approximately symmetric. At these longitudes, the dense torus extends about 10°-15° of latitude on either side of the equator. An animation of the run shown in Figure 2a is given in Supporting Information S1.

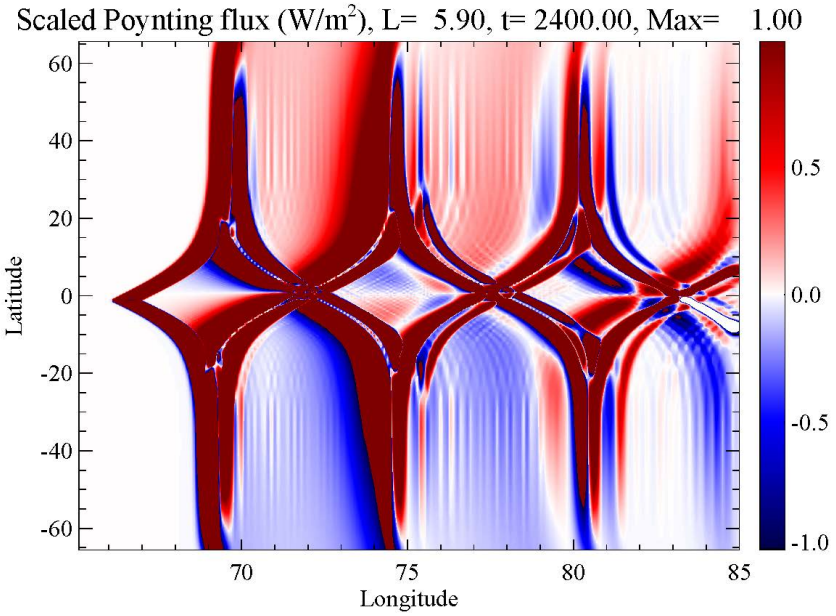

The reflections of the Alfvén wave at each ionosphere and at the torus boundary are very clear, as shown in illustrations of the wave propagation paths (e.g., Bonfond et al., 2008; Crary & Bagenal, 1997). By comparing the maximum Poynting flux in the torus with the Poynting flux just outside the torus, we estimate that 53% of the wave energy is transmitted through the torus boundary in the low-density case, while 64% is transmitted in the high-density case where the contrast in Alfvén speeds is less. These results are in contrast with the claim of Chust et al. (2005) that most of the power is reflected at this boundary and does not reach the Jovian atmosphere. Since Io moves at 0.46°/minute with respect to the co-rotating plasma (e.g., Hinton et al., 2019), the distance between the Main Alfvén Wing (MAW, using the terminology of Bonfond et al. (2013)) in one hemisphere and the Reflected Alfvén Wing (RAW) in the conjugate ionosphere is about 6° in the low-density case and 8° in the high-density case, consistent with the travel times noted above.

However, since the torus does not have a sharp boundary, there are minor reflections through the system. Weak waves propagating between each ionosphere and the near boundary of the torus can be seen, much like in Figure 2 of Crary and Bagenal (1997). Figure 3a shows the same data as in Figure 2a, but with the color bar saturated at 1 W/m^2 to bring out these weaker reflections. These show up particularly well in a map of the perpendicular electric field scaled to the ionosphere under the assumption that the field lines are equipotentials (Figure 3b). These secondary reflections appear to be stronger after the first reflected Alfvén wing. Although these waves are much weaker than the MAW, they still carry Poynting fluxes about 20 mW/m^2 in the low-density case. This can be compared with electron energy fluxes of 10 mW/m^2 downstream in the tail (Szalay et al., 2018). In addition, due to the very short travel time between the torus boundary and the nearer ionosphere, the reflections from the torus boundary and the ionosphere are very close together, so these two waves arrive almost simultaneously, smearing out the effect of the trailing spots. The Poynting flux decreases on each bounce due to the finite conductance of the ionosphere (1 S for this run) and the pattern becomes more complicated due to interference between the various bouncing waves.

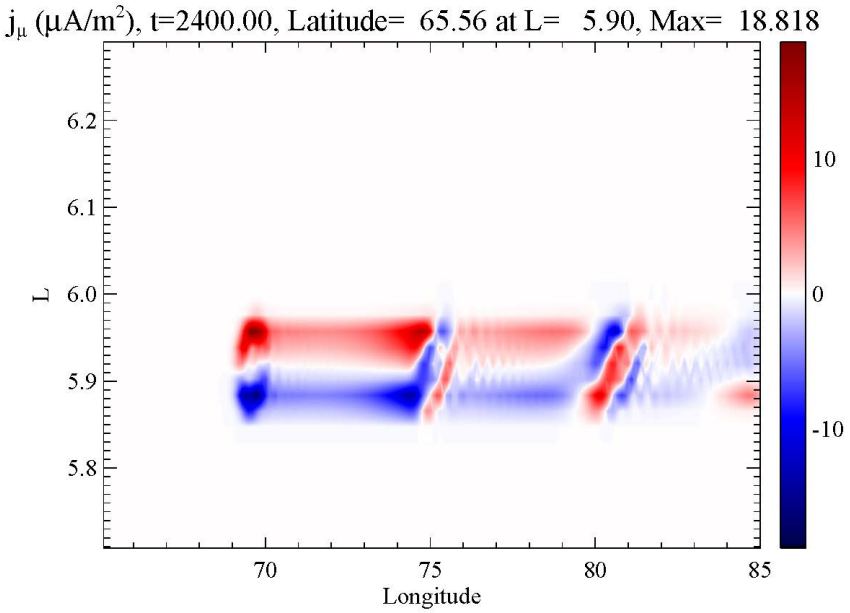

Figure 4 shows the field-aligned current patterns at the northern ionosphere for these two runs, with Figure 4a again showing the low-density case and Figure 4b the high-density case. In these plots, red color indicates northward (downward) current and blue indicates southward (upward) current. The currents are larger in the high-density case since more Alfvén wave power is transmitted through the torus. Since upward current is generally associated with auroral emissions, the blue spots are a proxy for the aurora in this figure (although it should be acknowledged that even downward current can be associated with counterstreaming fluxes that can produce aurora, as noted by Mauk et al., 2020). The current in the main Alfvén wing is the most intense current with the reflected wing (at 75° longitude) being the next most intense; however, there are weaker currents associated with the secondary reflections as well. (Note that the resolution of the simulation in the longitudinal direction is 0.1°, so that the small fluctuations are well resolved.)

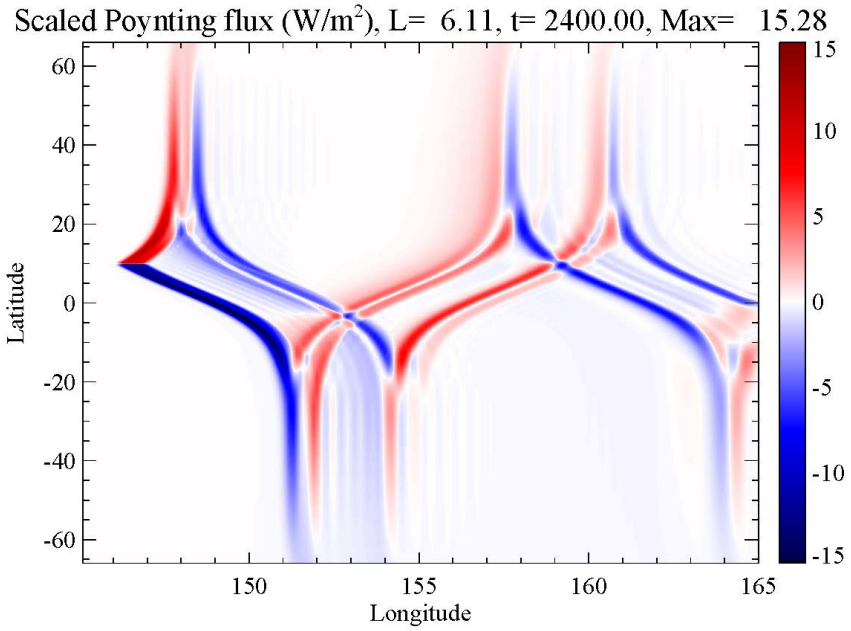

To interpret this figure, note that Io's diameter of 3644 km corresponds to 0.051 R_J and 0.49° of longitude. Using a dipole mapping, this corresponds to a footprint of about 140 km (0.11°) in latitude and 260 km in longitude. At a speed of 57 km/s, Io moves about one diameter in a minute. The field-aligned current at Io is generated at the Jupiter-facing edge and the edge on the far side from Jupiter (e.g., Saur et al., 2004), producing the U-shaped pattern seen in the figures. The current pattern oscillates back and forth with an amplitude of about 0.03 in L shell, which corresponds to a distance of 80 km, close to the 100 km transverse displacement seen by Mura et al. (2018). This pattern is apparently repeated about every 0.3° in the low-density model and 0.5° in the high-density model, implying a time scale for reflection of about 1 minute. Although Mura et al. (2018) state that specular reflection does not give this time scale for reflections off the torus, our full wave calculation suggests that reflections do return to the ionosphere on this time scale.

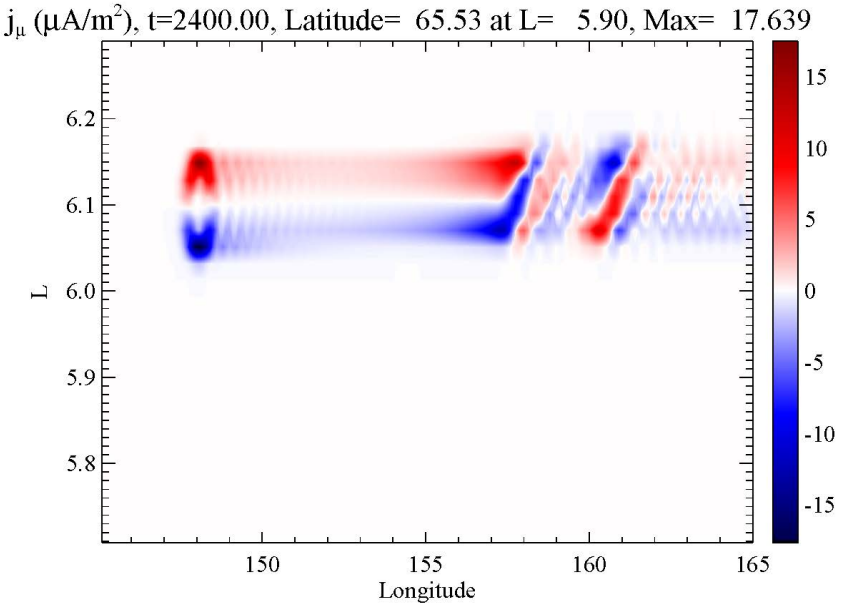

Between the arrival of the MAW and the RAW in each hemisphere, the currents are mainly on the side of Io closest to Jupiter (i.e., lower L-shell); however, after the passage of the RAW, the pattern becomes more complicated and the regions of upward current migrate across the footprint and appear at higher L-shells. This is due to phase mixing as the wave propagates. Phase mixing (e.g., Mann et al., 1995) occurs since the different field lines have slightly different lengths, so that Alfvén waves propagating on adjoining field lines become out of phase. This effect becomes more pronounced after the passage of the reflected Alfvén wing, which occurs after the Alfvén wave has passed through the whole plasma torus. At this point, the waves reflected from the torus boundary and from the conjugate ionosphere interfere with one another, producing the more complicated pattern as in the Poynting flux plot. Figure 4b for the high-density case shows similar features, with the MAW and RAW currents farther apart, as in Figure 2.

The situation is modified when Io is near the boundary of the torus. Figures 5a (low-density case) and 5b (high-density case) show the Poynting flux in the region where Io is at its most northerly latitude. In this case, the main Alfvén wing arrives at the northern ionosphere before the waves arrive at the southern ionosphere since they spend less time in the plasma torus. In this case, the MAW and RAW in the northern hemisphere are farther apart (about 9° of longitude) while they are closer together (3° of longitude) in the southern hemisphere. In addition, the reflection from the northern torus boundary and the northern ionosphere are very close together since both of these waves must traverse nearly the entire plasma torus. The secondary waves between the ionosphere and torus are weaker in the north and stronger in the south, particularly between the MAW and RAW in that hemisphere. This pattern is reversed between the hemispheres when Io is near the southern boundary of the torus (not shown). The run shown in Figure 5a is shown as an animation in Supporting Information S2.

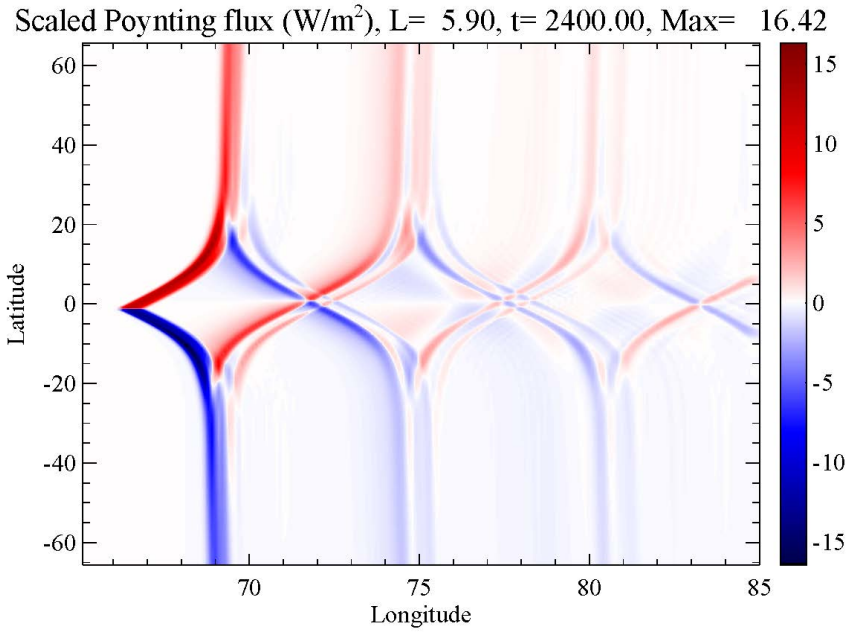

The currents at the ionosphere also show these features. Figures 6a and 6b show the field-aligned current in the northern ionosphere for the two cases, while Figures 6c and 6d show the corresponding currents in the southern ionosphere. Note that positive (red) field-aligned currents in both hemispheres are northward along the field line, so upward current in the southern hemisphere is red. The strongest currents in both hemispheres are associated with the RAW and MAW; however, there are weaker currents associated with the secondary waves. The currents are somewhat weaker than when Io is near the equator, and they are weaker in the southern hemisphere than in the north. As in the previous runs, the U shape of the main spot is due to the changing cross section of Io and its ionosphere as it crosses field lines; this structure is maintained in the reflected waves. This pattern is more distinct in the northern hemisphere currents, suggesting that the pattern is washed out to some degree passing through the plasma torus. In the northern hemisphere, the current pattern is similar to the symmetric case with the upward field-aligned current occurring at the lower L-shells; however, in the southern hemisphere the MAW and RAW spots are closer together with significant currents between them.

4 Ionospheric conductance effects

The model includes a height-integrated conductance in Jupiter's ionosphere. The runs presented so far all considered a Pedersen conductance of 1 S. However, Gérard et al. (2020) have used data from the Ultraviolet Spectral Imager (UVS) on Juno to make estimates of the Pedersen conductance, showing that it can range from 0.1 S to about 10 S, consistent with results from ionospheric modeling (Millward et al., 2002; Ray et al., 2014). We have done a series of runs to see the effect of the variation of the conductance at Jupiter, using the low-density model discussed above. Figure 7 shows the Poynting flux for runs in which Io is near the equator as in Figures 2a. Figure 7a shows the 0.1 S case, while Figure 7b gives the results for a Pedersen conductance of 10 S. In the low-conductance case, the ionosphere is closely matched to the Alfvén wave impedance and the wave is largely absorbed there. It can be seen that the reflection from the torus boundary is stronger than the reflection from the ionosphere. On the other hand, the reflection from the ionosphere in the 10 S case is very strong and does not lead to damping of the wave. In this case the secondary waves are enhanced compared to the lower conductance case.

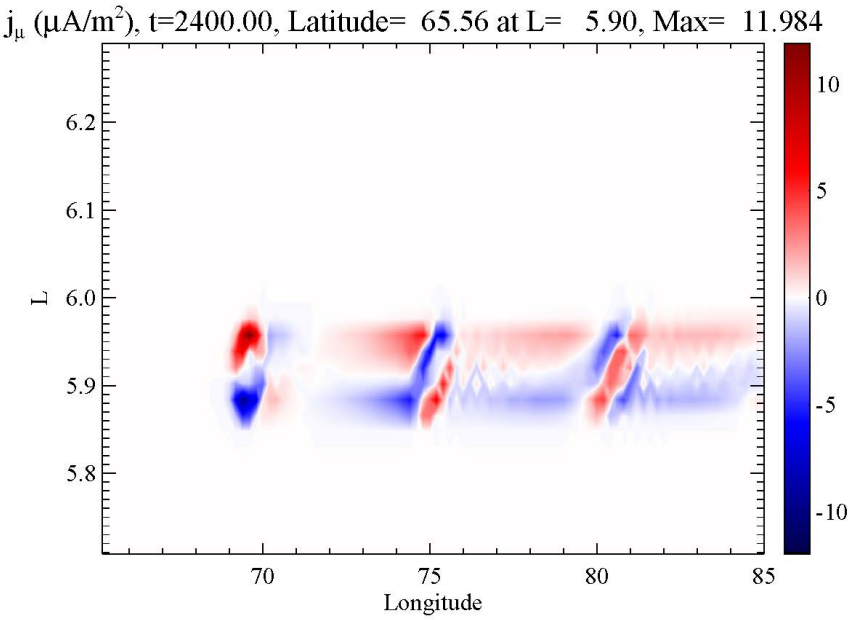

To quantify the amount of reflection in each case, we have decomposed the electric and magnetic fields into the so-called Elsässer variables (Elsässer, 1950), which for Alfvén waves can be written as , where the plus sign refers to waves propagating in the +μ direction (i.e., northward along the field line) and the minus sign to waves in the -μ direction. Evaluating these values at a latitude of 50° in the main Alfvén wing, we find that the reflection coefficients are 2.0%, 36.5% and 71.4% for the 0.1, 1.0 and 10.0 S cases, respectively. Mura et al. (2018) have shown that the tails can extend for over 100° in longitude around Jupiter. While these results favor a high Pedersen conductance, it is difficult to explain such extended tails even for the 10 S case.

The field-aligned currents at the ionosphere show similar characteristics. Figures 8a and 8b show the currents in the northern hemisphere for the runs shown in Figures 7a and 7b, respectively. A first point is that, unsurprisingly, the currents are stronger for higher conductance. The low conductance case shows a near absence of current between the MAW and RAW spots, and by the second reflected spot, the currents are much weaker. On the other hand, in the high conductance case the currents remain strong between the MAW and RAW, although still weaker than the MAW spot. In this case, there are strong reflections at both the ionosphere and the torus boundary. Reflections from the low Alfvén speed torus and the high conductance ionosphere both lead to reduction in the electric field and enhancement in the field-aligned current, leading to stronger currents even though the Poynting flux is low in between the main spots. In the high conductance case, the upward and downward currents are seen to switch positions due to multiple reflections and phase mixing as the waves propagate. These simulations suggest that a strong and relatively continuous current structure would be associated with high ionospheric conductance. This effect is possibly related to the bifurcated footprint seen far down the Io tail by Mura et al. (2018) and Szalay et al. (2018).

5 Parallel Electric Fields: Current limitation

The models described above only included the effects of electron inertia on the formation of parallel electric fields. Inertial electric fields are favored when the perpendicular wavelength is comparable to the electron inertial length. In the low-density model, the lowest density is 0.1 cm^{-3}, corresponding to an inertial length of 17 km; Io's radius of 1820 km mapped to the ionosphere is about 140 km, much larger than the inertial length. Therefore, the inertial fields are small, with the parallel fields integrated along the field line being the order of 500 volts. However, the resulting field-aligned currents can be very large, 15-20 μA/m^2 as can be seen in Figures 4 and 6. Kinetic modeling of the Io flux tube (Ray et al., 2009) indicates that such large

currents cannot be supported without the formation of large potential drops along the field lines. Thus, the effect of these parallel potential drops should be taken into account.

One difficulty in including this type of potential drop in the present model is that the Ray et al. (2009) formulation relates the field-aligned current to the total potential drop on the field line, while the present model includes the parallel electric field at each point along the field line. However, we can model this effect by including a current-limiting term in the equations. The maximum current that can be carried by a Maxwellian distribution with no bulk acceleration is for the case of a totally empty loss cone, i.e., a half-Maxwellian distribution with only one sign of the parallel velocity. In this case, the effective drift velocity is , where the electron temperature is given in electron volts. Thus, the maximum current is $j_{max} = nev_d$, which is 3.39 μA/m^2 for a density of 1 cm^{-3}and a temperature of 1 keV.

The parallel electric field can then be modeled by introducing the ν* term in the equation for the field-aligned current in equation . This term should be zero when the current is less thanj_{max} and increase rapidly as the current increases above this value. For this model, we choose the form

The parameter ν* is set to zero for weaker currents. The constant ν_0 can be estimated from the linear form of the Knight (1973) relation, $j = K\ \Phi$, where . The effective parallel conductivity is then $\sigma = KL$, where L is the distance over which the parallel field is distributed. Then we can write

Where L is in Jovian radii and we have again taken $n = 1$ cm^{-3} and $T_e = 1$keV. Thus, if we take this scale length to be about half a Jovian radius, we can conveniently set $\nu_0 = 1$ s^{-1}.

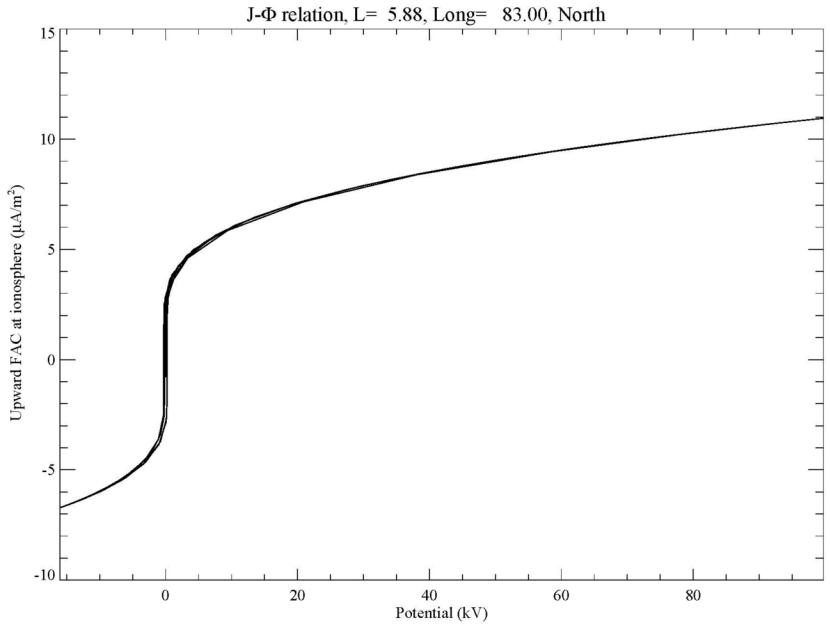

Figure 9 shows the resulting relationship between the parallel potential drop (more precisely, the integrated parallel electric field, since the field is not purely electrostatic) and the field-aligned current at the ionosphere with these parameters for a run that is otherwise the same as that shown in Figures 7b and 8b, which is the low-density case and a Pedersen conductance of 10 S at Jupiter. This figure shows the current-limiting effect of our model, with the currents being limited to about 10 μA/m^2 leading to potentials up to 100 kV. These parameters are consistent with the kinetic results of Ray et al. (2009), indicating that our model is a reasonable approximation to these results.

Figure 10a shows the field-aligned current from this run. The current pattern is spread out somewhat from the corresponding run without the parallel electric field (Figure 8b). Strong parallel electric fields lead to

a perpendicular component of the Poynting flux that broadens the magnetic perturbation. The amplitude of the magnetic perturbation fixes the total current that should flow in the flux tube, so that the current limitation requires the current to flow over a larger area. This leads to a splitting of the current pattern. In addition, the current is limited to about 10 $\mu A/m^2$ compared to almost twice that in Figure 9b. Figure 10b shows the parallel potential. The color bar in this figure has been limited to 25 kV to bring out some of the weaker potentials (the actual potential in the main spot is about 100 kV as in Figure 9. Note that in contrast to the field-aligned current plot, the red colors indicate regions of upward parallel electric field.

These figures show that while the main spots are accompanied by strong parallel electric fields, the secondary reflections of the wave from the torus boundary are not. This is largely due to the current-limiting nature of the current-voltage relation. This raises the question of how these auroral features in this region, as seen in the JIRAM data, are generated. It is likely that effects not included in our model, such as the filamentation of the currents due to nonlinear effects or feedback from the ionosphere, are important.

6 Discussion

This work has presented initial results from a full-wave model of the propagation of Io-related Alfvén waves through the Jovian magnetosphere. While this is an improvement upon earlier models involving ray-tracing or simplified box geometries, it still neglects a number of features that can affect the structure and dynamics of the Io-generated aurora. Most importantly, the acceleration of the auroral particles themselves is not modeled. For example, the model does not take into account the presence of the transhemispheric electron beams, thought to be produced by electrons accelerated by Alfvén waves in the torus itself. Nevertheless, a number of features in the observations of the Io tail may be understood by the model results.

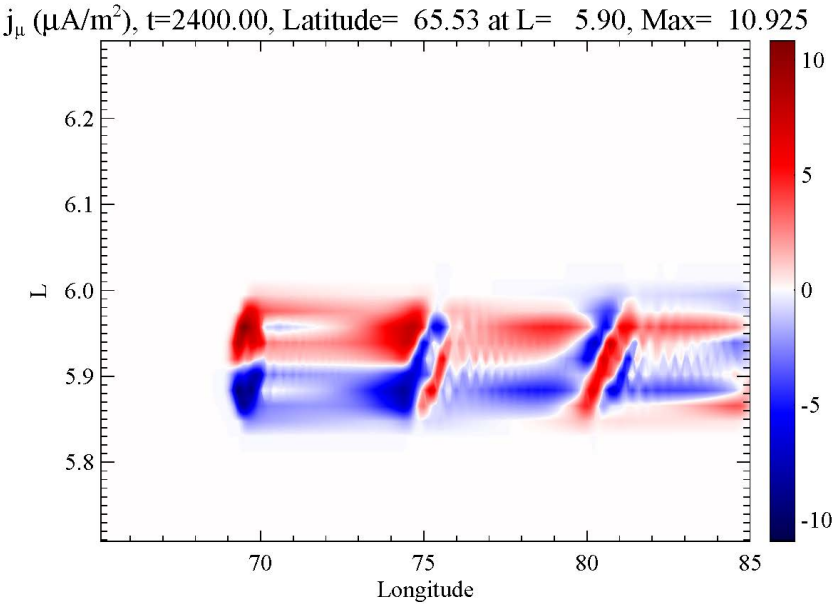

The overall structure of the main auroral spots is consistent with the expectations from ray-tracing models (e.g., Hinton et al., 2019). Our model indicates that the spacing of the main and reflected Alfvén wings is consistent with previous work and depends upon the density profile along the flux tube. Furthermore, the structure of the field-aligned currents produced by the model is consistent with the transverse displacement in secondary spots observed by JIRAM (Mura et al., 2018). The results suggest that this may be due to the generation of field-aligned currents at the surface of Io and its ionosphere. In addition, the secondary structure in the currents is consistent with the reflection of Alfvén waves from the boundary of plasma torus, which can occur over time scales of about a minute. However, one puzzle in the results is that when

the parallel electric fields due to current limitation are included, these secondary reflections do not produce significant potential drops.

The complicated structure after the passage of the RAW suggests that the waves are subject to phase mixing, particularly while passing through the dense plasma torus. This makes the current structure more complicated, especially after the passage of the reflected Alfvén wing. Recently, Schlegel and Saur (2022) considered the effect of different travel times on the alternating spots and concluded that this was only a minor effect. However, in our model, the difference in the passage time of an Alfvén wave from one ionosphere to another between L=5.90 and 5.95, a difference of about 1 Io radius, is 22.5 seconds in the low-density model and 30.6 seconds in high-density model, much larger than their assumed time of 3.7 seconds. In addition, the RAW spot occurs after the wave has traveled through the torus 1.5 times, so the difference is 50% larger. So it appears plausible that the travel time difference, i.e., phase mixing, can be an important effect down the tail from the main spot. This may be related to the bifurcated auroral tail sometimes seen downstream from main spot (Szalay et al., 2018; Mura et al., 2018).

In summary, this new model for the propagation of Alfvén waves generated by Io has revealed some interesting points and raised some questions about this interaction:

- The model confirms that reflections from the torus boundary are significant and give rise to the overall pattern of currents, indicating that the spacing of auroral emissions is dependent on the density along the flux tube. The transmission through the torus boundary is stronger in the high-density case since the density contrast is not as large, leading to higher currents at the ionosphere for this case.
- The Alfvén wave pattern depends strongly onthe position of Io within the plasma torus. The main and reflected Alfvén wings are farther apart and the magnitude of the currents is stronger in the northern hemisphere when Io is in this hemisphere.
- In addition to the main reflections, there are weaker secondary reflections of waves bouncing between Jupiter's ionosphere and the plasma torus. These may be responsible for the continued auroral emissions between the MAW and RAW spots. These secondary reflections appear to be particularly strong in the hemisphere opposite to the location of Io.
- The field-aligned currents due to the main Alfvén wing (MAW) have a characteristic U-shape due to the generation of field-aligned currents at the Jupiter-facing and anti-Jupiter side of Io. The repetition of this shape due to the secondary reflections may be related to the structure of the auroral emissions as seen by JIRAM (Mura et al., 2018).
- The length of the footprint tail is a function of the conductance in Jupiter's ionosphere. A conductance of 0.1 S leads to strong dissipation of the wave on each bounce, while for a 10 S conductance the waves can persist for many bounces. However, the tails extending over 100° in longitude reported by Mura et al. (2018) may require more than the linear propagation of the Alfvén waves.
- The currents produced by Io are strong enough to lead to potential drops of up to 100 kV along the main Alfvén wing. However, the current limitation due to these potential drops keeps the currents in the secondary reflections limited, so that it is not clear from the present work how particles are accelerated by these reflected waves.
- At long distances along the tail, phase mixing and the presence of multiple reflected waves can complicate the structure of the currents. For high conductance in the ionosphere, the upward and downward currents can reverse with the upward currents appearing on the high latitude side of the footprint.

While this model shows some interesting features, there are still many unanswered questions. Although our model includes the electron inertial effect thought to be responsible for the electric field producing a broadband electron distribution, there does not seem to be significant electric fields produced by this effect. This may be due to the large size of Juno with respect to the electron inertial length. However, if the currents are strongly filamented, the importance of the electron inertial effect would be increased. Including the possibility of a turbulent cascade to smaller scales (Hess et al., 2010; Saur et al., 2002) or ionospheric feedback effects (Lysak, 1991; Lysak and Song, 2002; Moirano et al., 2021) would give a more complete understanding of the propagation of Io-generated Alfvén waves in Jupiter's magnetosphere.

Acknowledgments

This research has benefited from discussions with Jamey Szalay, Licia Ray, Alessandro Mura and Alessandro Moirano. This work has been supported by by NASA Grant 80NSSC20K1269 to the University of Minnesota. A.H.S. acknowledges support from NASA NFDAP grant 80NSSC21K1242. The work at the University of Colorado was supported as a part of NASA's Juno mission, supported by NASA through contract 699050X with the Southwest Research Institute.

Open Research Section

The codes used to simulate the propagation of Alfvén waves generated by the Io interaction with Jupiter's magnetosphere as well as the IDL software used to display the data and produce the figures in this manuscript have been deposited in the Data Repository for the University of Minnesota (DRUM) at https://conservancy.umn.edu/handel/11299/166578.

References

Acuña, M. H., Neubauer, F. M., & Ness, N. F. (1981). Standing Alfven wave current system at Io - Voyager 1 observations. *Journal of Geophysical Research, 86* (A10), 8513–8521. http://doi.org/10.1029/JA086iA10p08513

Bagenal, F. (1983). Alfven wave propagation in the Io plasma torus.*Journal of Geophysical Research, 88* (A4), 3013–3025. https://doi.org/10.1029/JA088iA04p03013

Bagenal, F. & Dols, V. (2020) The space environment of Io and Europa,*Journal of Geophysical Research: Space Physics, 125,*e2019JA027485. https://doi.org/10.1029/2019JA027485

Belcher, J. W., Goertz, C. K., Sullivan, J. D., & Acuna, M. H. (1981). Plasma observations of the Alfven wave generated by Io. *Journal of Geophysical Research, 30,* 8508–8512. https://doi.org/10.1029/JA086iA10p08508

Bigg, E. K. (1964). Influence of the satellite Io on Jupiter's decametric emission. *Nature, 203* , 1008. https://doi.org/10.1038/2031008a0.

Bonfond, B. Grodent, D. Gerard, J.-C. Radioti, A. Dols, V. Delamere, P.A. & Clarke, J.T. (2009). The Io UV footprint: location, inter-spot distances and tail vertical extent. *J. Geophys. Res. 114,* 7224

Bonfond, B. Grodent, D. Gerard, J.-C. Radioti, A. Saur, J. Jacobsen, S. (2008). UV Io footprint leading spot: a key feature for understanding the UV Io footprint multiplicity? *Geophys. Res. Lett. 35* , 5107

Bonfond, B., Hess, S., Gerard, J.-C., Grodent, D., Radioti, A., Chantry, V., Saur, J., Jacobsen, S., & Clarke, J. T. (2013). Evolution of the Io footprint brightness I: Far-UV observations, *Planet. Space Sci., 88,* 64.

Chust, T., Roux, A., Kurth, W. S., Gurnett, D. A., Kivelson, M. G., & Khurana, K. K. (2005) Are Io's Alfven wings filamented? Galileo observations, *Planet. Space Sci., 53,* 395.

Clarke, J. T., Ajello, J., Ballester, G., Jaffel, L. B., Connerney, J., Gerard, J.-C., Gladstone, G R., Grodent, D., Pryor, W., Trauger, J., & Waite, J. H. (2002). Ultraviolet auroral emissions from the magnetic footprints of Io, Ganymede, and Europa on Jupiter, *Nature, 415.*997.

Clarke, J. T., Ballester, G. E., Trauger, J., Evans, R., Connerney, J. E. P., Stapelfeldt, K., et al. (1996). Far-ultraviolet imaging of Jupiter's aurora and the Io "footprint"'. *Science, 274* (5286), 404–409. https://doi.org/10.1126/science.274.5286.404

Connerney, J. E. P., Baron, R., Satch, T., & Owen T. (1993). Images of excited H_3^+ at the foot of the Io flux tube in Jupiter's Atmosphere, *Science, 262,* 1035.

Connerney, J. E. P., Kotsiaros, S.,Oliversen, R. J., Espley, J. R., Joergensen, J. L., Joergensen, P. S., et al. (2018). A new model of Jupiter's magnetic field from Juno's first nine orbits.*Geophysical Research Letters, 45,* 2590–2596. https://doi.org/10.1002/2018GL077312

Connerney, J. E. P., Timmins, S., Oliversen, R. J., Espley, J. R., Joergensen, J. L., Kotsiaros, S., et al. (2022). A new model of Jupiter's magnetic field at the completion of Juno's Prime Mission. Journal of Geophysical Research: Planets, 127, e2021JE007055. https://doi.org/10.1029/2021JE007055

Crary, F. J, & Bagenal, F. (1997). Coupling the plasma interaction at Io to Jupiter (1997). *Geophys. Res. Lett., 24,* 2135.

Dougherty L. P., Bodisch, K. M., & F. Bagenal (2017), Survey of Voyager plasma science ions at Jupiter: 2. Heavy ions, *J. Geophys. Res. Space Physics, 122,* doi:10.1002/2017JA024053.

Elsasser, W. M. (1950). The hydromagnetic equations, *Phys. Rev., 79,* 183.

Gerard, J.-C., Gkouvelis, L., Bonfond, B., Grodent, D., Gladstone, G. R., Hue, V., et al. (2020). Spatial distribution of the Pedersen conductance in the Jovian aurora from Juno-UVS spectral images.*Journal of Geophysical Research: Space Physics, 125* , e2020JA028142. https://doi.org/10.1029/2020JA028142

Goertz, C. (1980). Io's interaction with the plasma torus, *J. Geophys. Res., 85,* 2949-2956.

Gershman, D. J., Connerney, J. E. P., Kotsiaros, S., DiBraccio, G. A., Martos, Y. M., Vinas, A., et al. (2019). Alfvenic fluctuations associated with Jupiter's auroral emissions. *Geophysical Research Letters, 46.* https://doi.org/10.1029/2019GL082951

Goldreich, P. & Lynden-Bell, D. (1969). Io: a Jovian unipolar inductor,*Astrophys. J., 156,* 59.

Gurnett, D. A., & Goertz, C. K. (1981). Multiple Alfven wave reflections excited by Io: Origin of the Jovian decametric arcs. Journal of Geophysical Research, 86(A2), 717–722. https://doi.org/10.1029/JA086iA02p00717

Hinton, P. C., Bagenal, F., & Bonfond, B. (2019). Alfven wave propagation in the Io plasma torus. *Geophysical Research Letters, 46, 1* 242–1249. https://doi.org/10.1029/2018GL081472

Jacobsen, S., Neubauer, F. M., Saur, J., & Schilling, N. (2007). Io's nonlinear MHD-wave field in the heterogeneous Jovian magnetosphere. *Geophysical Research Letters, 34,* L10202. https://doi.org/10.1029/2006GL029187

Lysak, R. L., & Song, Y. (2020). Field line resonances in Jupiter's magnetosphere, *Geophysical Research Letters, 47,* e2020GL089473, https://doi.org/10.1029/2020GL089473

Lysak, R. L., Song, Y., Elliott, S., Kurth, W., Sulaiman, A. H., & Gershman, D. (2021). The Jovian ionospheric Alfven resonator and auroral particle acceleration. *Journal of Geophysical Research: Space Physics, 126* , e2021JA029886. https://doi.org/10.1029/2021JA029886

Lysak, R. L., Song, Y., Sciffer, M. D., & Waters, C. L. (2015), Propagation of Pi2 pulsations in a dipole model of the magnetosphere*, J. Geophys. Res. Space Physics, 120,*doi:10.1002/2014JA020625.

Lysak, R. L., Song, Y., Waters, C. L., Sciffer, M. D., & Obana, Y. (2020). Numerical investigations of interhemispheric asymmetry due to ionospheric conductance. *Journal of Geophysical Research: Space Physics, 125,* e2020JA027866. https://doi.org/10.1029/2020JA027866

Mann, I. R., Wright, A. N., & Cally, P. S. (1995), Coupling of magnetospheric cavity modes to field line resonances: a study of resonant widths,*J. Geophys. Res., 100,* 19,441.

Mauk, B. H., Clark, G., Gladstone, G. R., Kotsiaros, S., Adriani, A., Allegrini, F., et al. (2020). Energetic particles and acceleration regions over Jupiter's polar cap and main aurora: A broad overview. Journal of Geophysical Research: Space Physics, 125, e2019JA027699. https://doi.org/10.1029/2019JA027699

Millward, G., Miller, S., Stallard, T., Aylward, A. D., & Achilleos, N. (2002). On the dynamics of the Jovian ionosphere and thermosphere. III. The modeling of auroral conductivity, Icarus, 160, 95-107. https://doi.org/10.1006/icar.2002.6951

Moirano, A., Mura, A., Adriani, A., Dols, V., Bonfond, B., Waite, J. H., et al. (2021). Morphology of the auroral tail of Io, Europa, and Ganymede from JIRAM L-band imager. *Journal of Geophysical Research: Space Physics, 126,* e2021JA029450. https://doi.org/10.1029/2021JA029450

Mura, A., Adriani, A., Altieri, F., Connerney, J. E. P., Bolton, S. J., Moriconi, M. L., et al. (2017). Infrared observations of Jovian aurora from Juno's first orbits: Main oval and satellite footprints: Jovian aurora IR observations from Juno. Geophysical Research Letters, 44(11), 5308–5316. https://doi.org/10.1002/2017GL072954

Mura, A., Adriani, A., Connerney, J. E. P., Bolton, S., Altieri, F., Bagenal, F., et al. (2018). Juno observations of spot structures and a split tail in Io-induced aurorae on Jupiter, *Science, 361,*774-777. https://doi.org/10.1126/science.aat1450

Neubauer, F. M. (1980). Nonlinear standing Alfven wave current system at Io: Theory, *J. Geophys. Res., 85,* 1171-1178.

Ray, L. C., Achilleos, N. A., M. F. Vogt, and J. N. Yates (2014), Local time variations in Jupiter's magnetosphere-ionosphere coupling system, J. Geophys. Res. Space Physics, 119, 4740–4751, doi:10.1002/2014JA019941.

Ray, L. C., Su, Y.-J., Ergun, R. E., Delamere, P. A. & Bagenal, F. (2009), Current-voltage relation of a centrifugally confined plasma,*J. Geophys. Res., 114,* A04214, doi:10.1029/2008JA013969.

Saur, J. (2004). A model of Io's local electric field for a combined Alfvenic and unipolar inductor far-field coupling. *Journal of Geophysical Research, 109,* A01210. https://doi.org/10.1029/2002JA009354

Schlegel, S., & Saur, J. (2022). Alternating emission features in Io's footprint tail: magnetohydrodynamical simulations of possible causes.*Journal of Geophysical Research: Space Physics, 127,*e2021JA030243. https://doi.org/10.1029/2021JA030243

Sulaiman, A. H., Hospodarsky, G. B., Elliott, S. S., Kurth, W. S., Gurnett, D. A., Imai, M., et al. (2020). Wave-particle interactions associated with Io's auroral footprint: Evidence of Alfven, ion cyclotron, and whistler modes. *Geophysical Research Letters, 47,*e2020GL088432. https://doi.org/10.1029/2020GL088432

Szalay, J. R., Bagenal, F., Allegrini, F., Bonfond, B., Clark, G., Connerney, J. E. P., et al. (2020). Proton acceleration by Io's Alfvenic interaction. *Journal of Geophysical Research: Space Physics, 125* , e2019JA027314. https://doi.org/10.1029/2019JA027314

Szalay, J. R., Bonfond, B., Allegrini, F., Bagenal, F., Bolton, S., Clark, G.. et al. (2018), In situ observations connected to the Io footprint tail aurora, *J. Geophys. Res.: Planets, 123,* 3061, doi: https://doi.org/10.1029/2018JE005752

Takahashi, K., Lysak, R., & Vellante, M. (2022). Statistical analysis of Pi2 pulsations observed by Van Allen Probes. *Journal of Geophysical Research: Space Physics, 127,* e2022JA030674. https://doi.org/10.1029/2022JA030674

Takahashi, K., Lysak, R. L., Vellante, M., Kletzing, C. A., Hartinger, M. D., & Smith, C. W. (2018), Observation and numerical simulation of cavity mode oscillations excited by an interplanetary shock, *J. Geophys. Res. Space Physics, 123* , 1969, doi: 10.1002/2017JA024639.

Open Research

AGU requires an Availability Statement for the underlying data needed to understand, evaluate, and build upon the reported research at the time of peer review and publication. Additionally, authors should include an Availability Statement for the software that has a significant impact on the research. Details and templates are in the*Availability Statement* section of the Data & Software for Authors Guidance. For physical samples, use the IGSN persistent identifier, see the*International Geo Sample Numbers* section.

References

References in supporting information must also be included in the reference list of the main paper, or in a designated section in the main paper so that they will be discovered, linked, and indexed. A separate list in the supporting information is not necessary. References are not included in word counts for excess length fees.

In the References section, cite the data/software described in the Availability Statement (this includes primary and processed data used for your research). For details on data/software citation as well as examples, see the*Data & Software Citation* section of the Data & Software for Authors guidance.

All references must be available to readers at the time of publication; there should be no "unpublished", in preparation, under review, or "in press" references. Please write the respective journal with any questions.

An example of a reference:

Deng, A., & Stauffer, D. R. (2006), On improving 4-km mesoscale model simulations. *Journal of Applied Meteorology and Climatology* ,*45* (3), 361–381. doi:10.1175/JAM2341.1

More information on reference formatting with examples can be found in our*Brief Guide to AGU Style*.

Figure 1. The figure caption should begin with an overall descriptive statement of the figure followed by additional text. They should be immediately after each figure. Figure parts are indicated with lower-case letters (a, b, c. . .). For initial submission, please place both the figures and captions in the text near where they are cited rather than at the end of the file (not both). At revision, captions can be placed in-text or at the end of the file, and figures should be uploaded separately. Each figure should be one complete, cohesive file (please do not upload sub-figures or figure parts in separate files). Data that supports the figure must be preserved in a repository, included in the Open Research section, and cited in the References. Include detailed information on how to recreate the figure in support of transparency (e.g., Python, R library).

Table 1. Start this caption with a short description of your table. Format tables using the Word Table commands and structures. Additional information on table formatting can be found in our Style Guide,

Table Formatting. **Do not create tables using spaces or tab characters. Large tables should not be included in the main text of the paper, but instead preserved as a .csv file in a repository. All data displayed in tables must be preserved in a repository, included in the Open Research section, and cited in the References.**

Figure 1 . The figure caption should begin with an overall descriptive statement of the figure followed by additional text. They should be immediately after each figure. Figure parts are indicated with lower-case letters (**a, b, c. . .**). For initial submission, please place both the figures and captions in the text near where they are cited rather than at the end of the file (not both). At revision, captions can be placed in-text or at the end of the file, and figures should be uploaded separately. Each figure should be one complete, cohesive file (please do not upload sub-figures or figure parts in separate files).

Table 1. Start this caption with a short description of your table. Format tables using the Word Table commands and structures. Additional information on table formatting can be found in our Style Guide, Table Formatting. Do not create tables using spaces or tabs characters. Large tables presenting rich data should be presented as separate excel or .csv files, not as part of the main text.

Hosted file

`Io paper supporting info.docx` available at https://authorea.com/users/523687/articles/611147-a-numerical-model-for-the-interaction-of-io-generated-alfv%C3%A9n-waves-with-jupiter-s-magnetosphere-and-ionosphere

A Numerical Model for the Interaction of Io-Generated Alfvén Waves with Jupiter's Magnetosphere and Ionosphere

R. L. Lysak[1], A. H. Sulaiman[1], F. Bagenal[2], F. Crary[2]

[1]School of Physics and Astronomy, Minnesota Institute for Astrophysics, University of Minnesota, Minneapolis, MN; [2]Laboratory for Astrophysics and Space Physics, University of Colorado, Boulder, CO

Corresponding author: Robert L. Lysak (lysak001@umn.edu)

Key Points:

- The spacing of the main auroral spots in Io's footprint tail depends on the density profile assumed as well as the magnetic latitude of Io.
- Partial reflections at the boundary of the Io plasma torus lead to secondary reflections and weaker auroral spots between the main spots.
- The length of the auroral tail depends on the ionospheric conductance at Jupiter, with higher conductances leading to longer tails.

Abstract

The interaction of Io with the co-rotating magnetosphere of Jupiter is known to produce Alfvén wings that couple the moon to Jupiter's ionosphere. We present first results from a new numerical model to describe the propagation of these Alfvén waves in this system. The model is cast in magnetic dipole coordinates and includes a dense plasma torus that is centered around the centrifugal equator. Results are presented for two density models, showing the dependence of the interaction on the magnetospheric density. Model results are presented for the case when Io is near the centrifugal and magnetic equators as well as when Io is at its northernmost magnetic latitude. The effect of the conductance of Jupiter's ionosphere is considered, showing that a long auroral footprint tail is favored by high Pedersen conductance in the ionosphere. The current patterns in these cases show a U-shaped footprint due to the generation of field-aligned current on the Jupiter-facing and Jupiter-opposed sides of Io, which may be related to the structure in the auroral footprint seen in the infrared by Juno. A model for the development of parallel electric fields is introduced, indicating that the main auroral footprints of Io can generate parallel potentials of up to 100 kV.

Plain Language Summary

Jupiter's moon Io generated electrical currents when it passes through Jupiter's magnetic field. These currents take the form of fluctuations in the magnetic field lines, much like the waves on a stringed musical instrument. Due to the motion of Io, these waves follow behind Io and bounce back and forth between Jupiter and the dense ionized gas emitted by Io. This process creates auroral emissions that can be observed, for example, with the Hubble Space Telescope.

1 Introduction

Alfvén waves have long been associated with the coupling of the moon Io with the ionosphere of Jupiter since the discovery by Bigg (1964) that the Jovian decametric radio emissions were modulated by the phase of Io in its orbit. Goldreich and Lynden-Bell (1969) identified Io as the generator of field-aligned current due to its motion relative to the co-rotating plasma at Jupiter. Goertz (1980) and Neubauer (1980) noted that this is due to the launching of Alfvén "wings" from the moving satellite. These Alfvén waves were identified by the Voyager 1 flyby of Jupiter (Acuña et al., 1981; Belcher et al., 1981). The reflection of these Alfvén waves from Jupiter's ionosphere was invoked by Gurnett and Goertz (1981) to explain the multiplicity of decametric radio emissions. The role of the plasma torus produced by the volcanic activity on Io at modifying the propagation of Alfvén waves was recognized by Bagenal (1983), who considered the reflecting Alfvén wave model in the context of plasma measurements from the Voyager mission. She noted that the travel time for Alfvén waves to propagate from Io to Jupiter depended on Io's position with respect to the plasma torus, which peaks at the centrifugal equator (i.e., the loci of points on each field line that is farthest from the rotation axis of Jupiter) at a angle of 7° from Io's orbital plane. The auroral emissions from Io were observed from the Infrared Telescope Facility (Connerney et al., 1993) and the Hubble Space Telescope (Bonfond et al., 2008, 2009; Clarke et al., 1996, 2002). The pre-Juno understanding of the Io-plasma interaction was summarized by Saur et al. (2004) and Bagenal and Dols (2020).

With the arrival of the Juno satellite at Jupiter in July, 2016, detailed measurements of particles and waves in Jupiter's magnetosphere became possible. In particular, the Juno orbit has made a number of high-latitude crossings of field lines magnetically connected to Io, indicating the presence of accelerated electrons and ions (Szalay et al., 2018, 2020) and Alfvén waves with a power law spectrum extending up to the proton gyrofrequency (Gershman et al., 2019; Sulaiman et al., 2020). Observations of the Io footprint tail have been made by the Jovian Infrared Auroral Mapper (JIRAM) instrument on Juno (Moirano et al., 2021; Mura et al., 2017, 2018), which indicate that the footprint tail is made up from a series of spots that at times appear to alternate positions with respect to the footprint of Io's orbit. The purpose of the present work is to show the first results from a numerical model of the Io interaction with Jupiter's magnetosphere and ionosphere to help understand this interaction.

The propagation of these Alfvén waves was considered qualitatively by Crary and Bagenal (1997) as well as Bonfond et al. (2008). More recently, Hinton et al. (2019) used a diffusive equilibrium model of the plasma density to construct ray paths for the reflecting Alfvén waves. On the other hand, Crary and Bagenal (1997) and Jacobsen et al. (2007) assumed a sharp gradient and straight magnetic field lines. A new model for the interaction of Io was introduced by Schlegel and Saur (2022) who used a Hall-MHD model to describe the interaction. They included the Hall conductivity in Io's ionosphere in an attempt to understand the alternating auroral spots observed by Mura et al. (2018) and Moirano et al. (2021). However, this model apparently assumed perfect

conductivity in the Jovian ionosphere and straight magnetic field lines.

In order to improve upon these earlier efforts, we have developed a model for the propagation of Alfvén waves from Io that is cast in a more realistic dipole geometry. We note that the orbit of Io is roughly in the equatorial plane of Jupiter, while the magnetic dipole moment is displaced by 10.25°, consistent with the dipole term in the spherical harmonic analysis of JRM33 (Connerney et al., 2022). (It should be noted that this tilt is 9.52° for the VIP4 model (Connerney et al., 1998) and 10.31° for the JRM09 model (Connerney et al., 2018); however, the results presented here are not too sensitive to the magnetic field model used.) The Io plasma torus is centered on the centrifugal equator, which is two-thirds of the distance from the rotational equatorial plane to the magnetic equatorial plane (e.g., Bagenal, 1983). Io is modeled as a cloud of Pedersen conductivity that is moving with respect to the co-rotating plasma of Jupiter's magnetosphere. Jupiter's ionospheres are modeled by a height-integrated Pedersen conductance. In this work, we will focus on the effects of the plasma distribution along the Io flux tube as well as the effect of different conductances on the field-aligned current signatures from Io. The next section will describe the model, followed by a discussion of the effect of the density profile. The following section will consider variations in the conductance of Jupiter's ionosphere. Then the effect of parallel electric fields due to kinetic effects will be considered. We will conclude with a discussion of the implications of these results for the structure of the auroral footprint tail of Io.

2 Model Description

The model presented here is the latest version of a series of models to describe the propagation of Alfvén waves in magnetospheric geometries. Previous versions of this model have been used in the magnetosphere of Earth, where it has been used to describe the structure of field line resonances and cavity modes in response to the propagation of Pi2 pulsations (Lysak et al., 2015; Takahashi et al., 2022), interplanetary shock impacts (Takahashi et al., 2018) and the excitation of quarter-wave modes due to interhemispheric asymmetry in the ionosphere (Lysak et al., 2020). Versions of this model have also been used to study field line resonances at Jupiter (Lysak & Song, 2020) and the effect of the ionospheric Alfvén resonator at Jupiter (Lysak et al., 2021). The model is cast into magnetic dipolar coordinates, defined in terms of magnetic spherical coordinates by

Here is the negative inverse of the L-shell parameter and points outwards (we will use L-shell in this paper rather than the M-shell used when non-dipolar fields are important to indicate that we are using a dipolar geometry, which is a reasonable approximation at the orbit of Io), is the magnetic east longitude, defined so that it corresponds with System III Right-Handed coordinates at the points where Juno crosses the magnetic equator, and is a field-aligned coordinate, proportional to the magnetic scalar potential of the dipole field. This coordinate increases from south to north, opposite the direction of the Jovian magnetic field. Note that we will use east longitudes throughout this

paper, although west longitudes are often used by Earth-based observers since the west longitude increases with time as seen from Earth as Jupiter rotates. For simplicity, we consider only the shear Alfvén mode; however, we can include the effect of parallel electric fields due to electron inertia or kinetic effects. In this case the relevant electrodynamic equations are

Here we have introduced the scale factors , and , where $R_J = 71492$ km is the equatorial radius of Jupiter, $B_J = 417.7$ T is the equatorial dipole magnetic field at the surface of Jupiter according to JRM33 (this value is 426.4 T for the VIP4 model and 419.9 T for JRM09). We use where is the non-relativistic Alfvén speed to denote the Alfvén speed including the displacement current. The coefficient * is a parameter to characterize the kinetic effects (such as the development of double layers) that can lead to parallel electric fields in strong current regions. This parameter will be set to zero until the last section of this manuscript.

The equations are modeled in a frame co-rotating with Jupiter's magnetosphere. In this frame, Io moves westward at a speed of 57 km/s, leading to an emf of $V_{Io}B_0$ of 120 mV/m. This effect is included in the second term in the equation for E in equation . Io is modeled as a cloud of conductivity which is constant over the diameter of Io and falls off as the distance squared in Io's ionosphere. As noted above, the simulation is based on magnetic coordinates, so that Io moves in a plane inclined about 10° from the magnetic equator. Similarly, the mass density in the Io plasma torus is centered on the centrifugal equator. We use two density profiles: a "high-density" case based on the density model of Dougherty et al. (2017), and a "low-density" case based on the model considered by Ray et al. (2009). These densities are taken to be independent of longitude along the centrifugal equator. The density and the resulting Alfvén speed c_A are plotted in Figure 1, with Figures 1a and 1b giving the density for the low- and high-density cases, respectively,

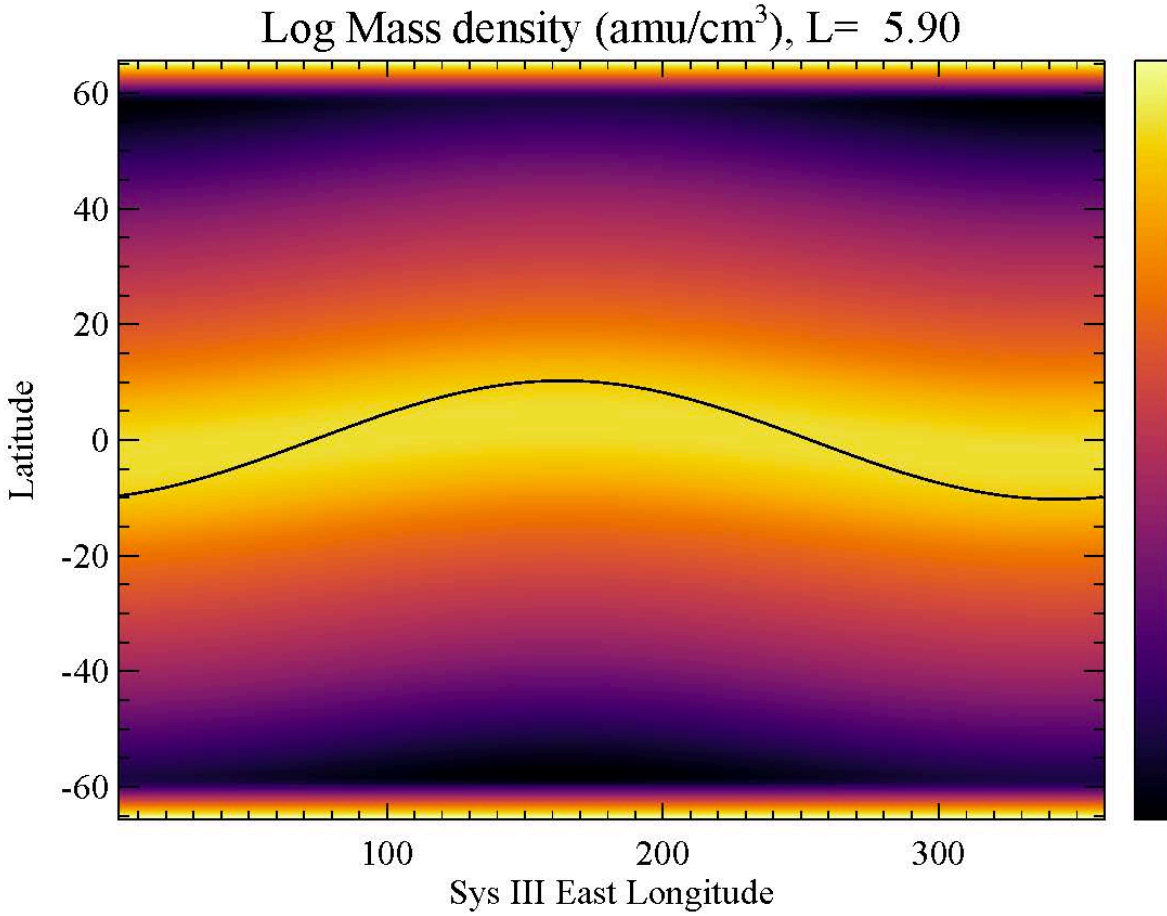

Figures 1c and 1d show the corresponding Alfvén speed profiles. The high-density case results in a density of 200 cm^{-3} at a radial distance of 2 R_J, while the low-density case has 0.1 cm^{-3} at this altitude. The trajectory of Io in magnetic coordinates is plotted as a solid line in these figures. These models have a total Alfvén transit time from one ionosphere to the other of 16 minutes in the high-density case and 12 minutes in the low-density case. These values are comparable to the one-way transit times between 12.5 and 15 minutes in the model of Hinton et al. (2019).

3 Results: Effects of density model and longitude

With this numerical model, we can simulate the propagation of Alfvén

waves from Io at various points along Io's orbit. First, consider a case where Io is near the centrifugal equator, so that the Alfvén travel times from Io to each hemisphere are approximately the same. The Pedersen

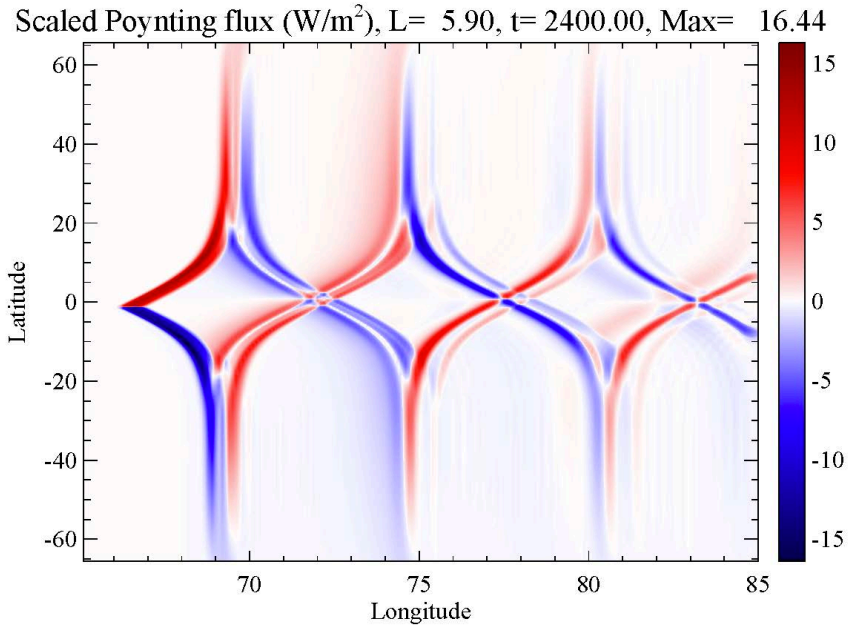

conductance of both ionospheres is set at 1 mho for these runs. Figure 2 shows the parallel component of the wave Poynting flux for such a case, 40 minutes from the start of the run. Io starts at 85° longitude (at the right side of the figure) and propagates westward. Note that Io crosses the centrifugal and magnetic equators at 74.3°. In this figure, red colors indicate northward Poynting flux while blue colors indicate southward flux, with the intensity of the colors indicating the magnitude. The magnitude of the Poynting flux is scaled by the background magnetic field to account for the smaller flux tube radius as the wave approaches each ionosphere. Figure 2a shows the results from the low-density case, while the high-density case is given in Figure 2b. As expected, the northern and southern wave patterns are approximately symmetric. At these longitudes, the dense torus extends about 10°-15° of latitude on either side of the equator. An animation of the run shown in Figure 2a is given in Supporting Information S1.

The reflections of the Alfvén wave at each ionosphere and at the torus boundary are very clear, as shown in illustrations of the wave propagation paths (e.g., Bonfond et al., 2008; Crary & Bagenal, 1997). By comparing the maximum Poynting flux in the torus with the Poynting flux just outside the torus, we estimate that 53% of the wave energy is transmitted through the torus boundary in the low-density case, while 64% is transmitted in the high-density case where the contrast in Alfvén speeds is less. These results are in contrast with the claim of Chust et al. (2005) that most of the power is reflected at this boundary

and does not reach the Jovian atmosphere. Since Io moves at 0.46°/minute with respect to the co-rotating plasma (e.g., Hinton et al., 2019), the distance between the Main Alfvén Wing (MAW, using the terminology of Bonfond et al. (2013)) in one hemisphere and the Reflected Alfvén Wing (RAW) in the conjugate ionosphere is about 6° in the low-density case and 8° in the high-density case, consistent with the travel times noted above.

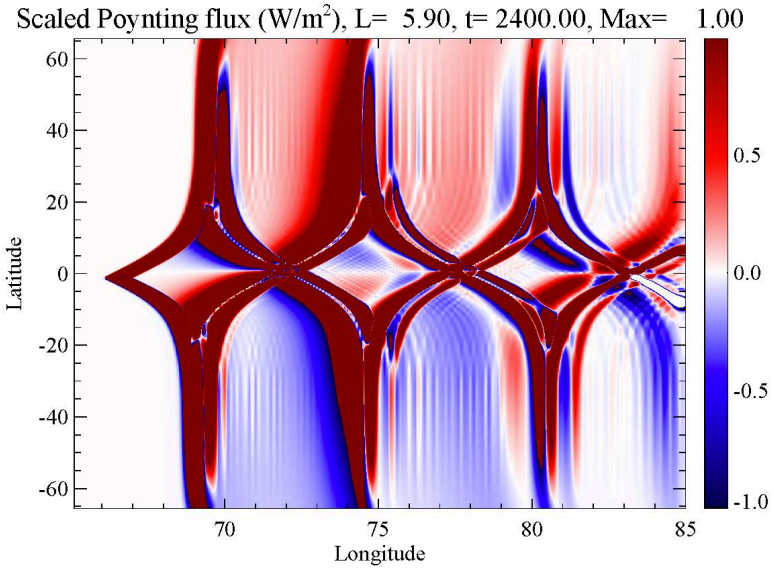

However, since the torus does not have a sharp boundary, there are minor reflections through the system. Weak waves propagating between each ionosphere and the near boundary of the torus can be seen, much like in Figure 2 of Crary and Bagenal (1997). Figure 3a shows the same data as in Figure 2a, but with the color bar saturated at 1 W/m^2 to bring out these weaker reflections. These show up particularly well in a map of the perpendicular electric field scaled to the ionosphere under the assumption that the field lines are equipotentials (Figure 3b). These secondary reflections appear to be stronger after the first reflected Alfvén wing. Although these waves are much weaker than the MAW, they still carry Poynting fluxes about 20 mW/m^2 in the low-density case. This can be compared with electron energy fluxes of 10 mW/m^2 downstream in the tail (Szalay et al., 2018). In addition, due to the very short travel time between the torus boundary and the nearer ionosphere, the reflections from the torus boundary and the ionosphere are very close together, so these two waves arrive almost simultaneously, smearing out the effect of the trailing spots. The Poynting flux decreases on each bounce due to the finite conductance of the ionosphere (1 S for this run) and the pattern becomes more complicated due to interference between the various bouncing waves.

Figure 4 shows the field-aligned current patterns at the northern ionosphere for these two runs, with Figure 4a again showing the low-density case

and Figure 4b the high-density case. In these plots, red color indicates northward (downward) current and blue indicates southward (upward) current. The currents are larger in the high-density case since more Alfvén wave power is transmitted through the torus. Since upward current is generally associated with auroral emissions, the blue spots are a proxy for the aurora in this figure (although it should be acknowledged that

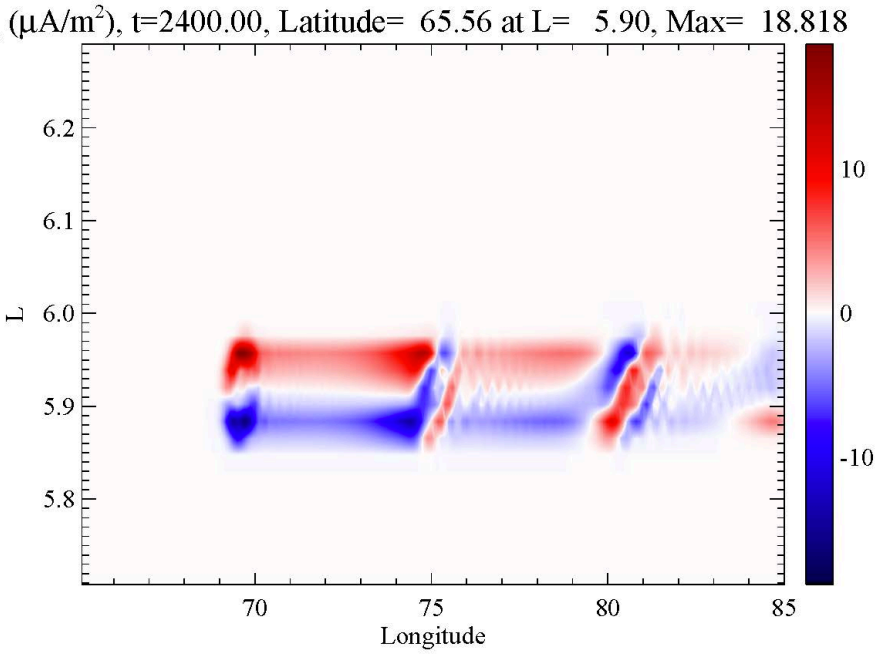

even downward current can be associated with counterstreaming fluxes that can produce aurora, as noted by Mauk et al., 2020). The current in the main Alfvén wing is the most intense current with the reflected wing (at 75° longitude) being the next most intense; however, there are weaker currents associated with the secondary reflections as well. (Note that the resolution of the simulation in the longitudinal direction is 0.1°, so that the small fluctuations are well resolved.)

To interpret this figure, note that Io's diameter of 3644 km corresponds to 0.051 R_J and 0.49° of longitude. Using a dipole mapping, this corresponds to a footprint of about 140 km (0.11°) in latitude and 260 km in longitude. At a speed of 57 km/s, Io moves about one diameter in a minute. The field-aligned current at Io is generated at the Jupiter-facing edge and the edge on the far side from Jupiter (e.g., Saur et al., 2004), producing the U-shaped pattern seen in the figures. The current pattern oscillates back and forth with an amplitude of about 0.03 in L shell, which corresponds to a distance of 80 km, close to the 100 km transverse displacement seen by Mura et al. (2018). This pattern is apparently repeated about every 0.3° in the low-density model and 0.5° in the high-density model, implying a time scale for reflection of about 1 minute. Although Mura et al. (2018)

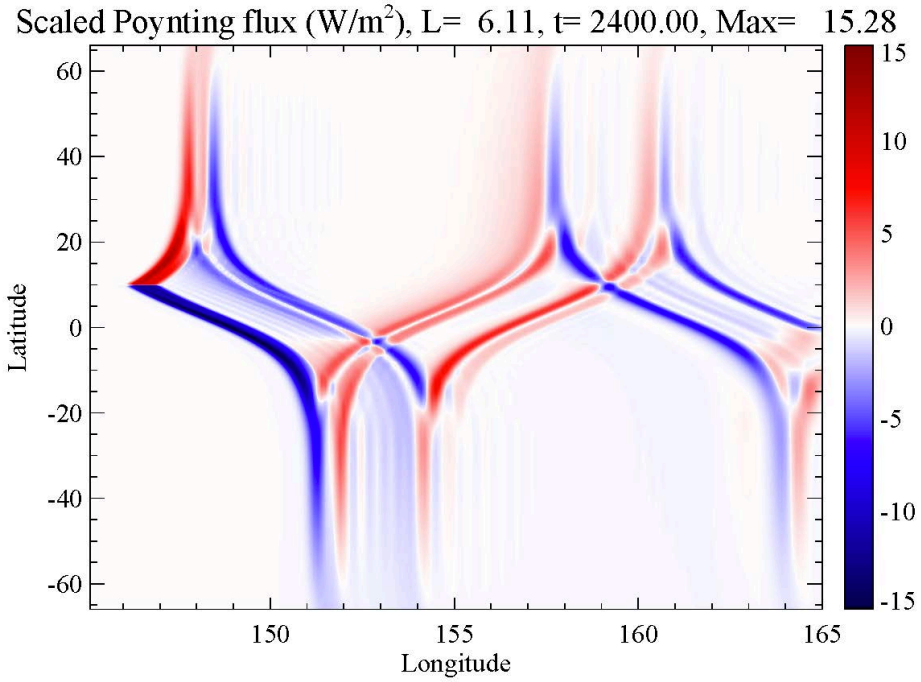

state

that specular reflection does not give this time scale for reflections off the torus, our full wave calculation suggests that reflections do return to the ionosphere on this time scale.

Between the arrival of the MAW and the RAW in each hemisphere, the currents are mainly on the side of Io closest to Jupiter (i.e., lower L-shell); however, after the passage of the RAW, the pattern becomes more complicated and the regions of upward current migrate across the footprint and appear at higher L-shells. This is due to phase mixing as the wave propagates. Phase mixing (e.g., Mann et al., 1995) occurs since the different field lines have slightly different lengths, so that Alfvén waves propagating on adjoining field lines become out of phase. This effect becomes more pronounced after the passage of the reflected Alfvén wing, which occurs after the Alfvén wave has passed through the whole plasma torus. At this point, the waves reflected from the torus boundary and from the conjugate ionosphere interfere with one another, producing the

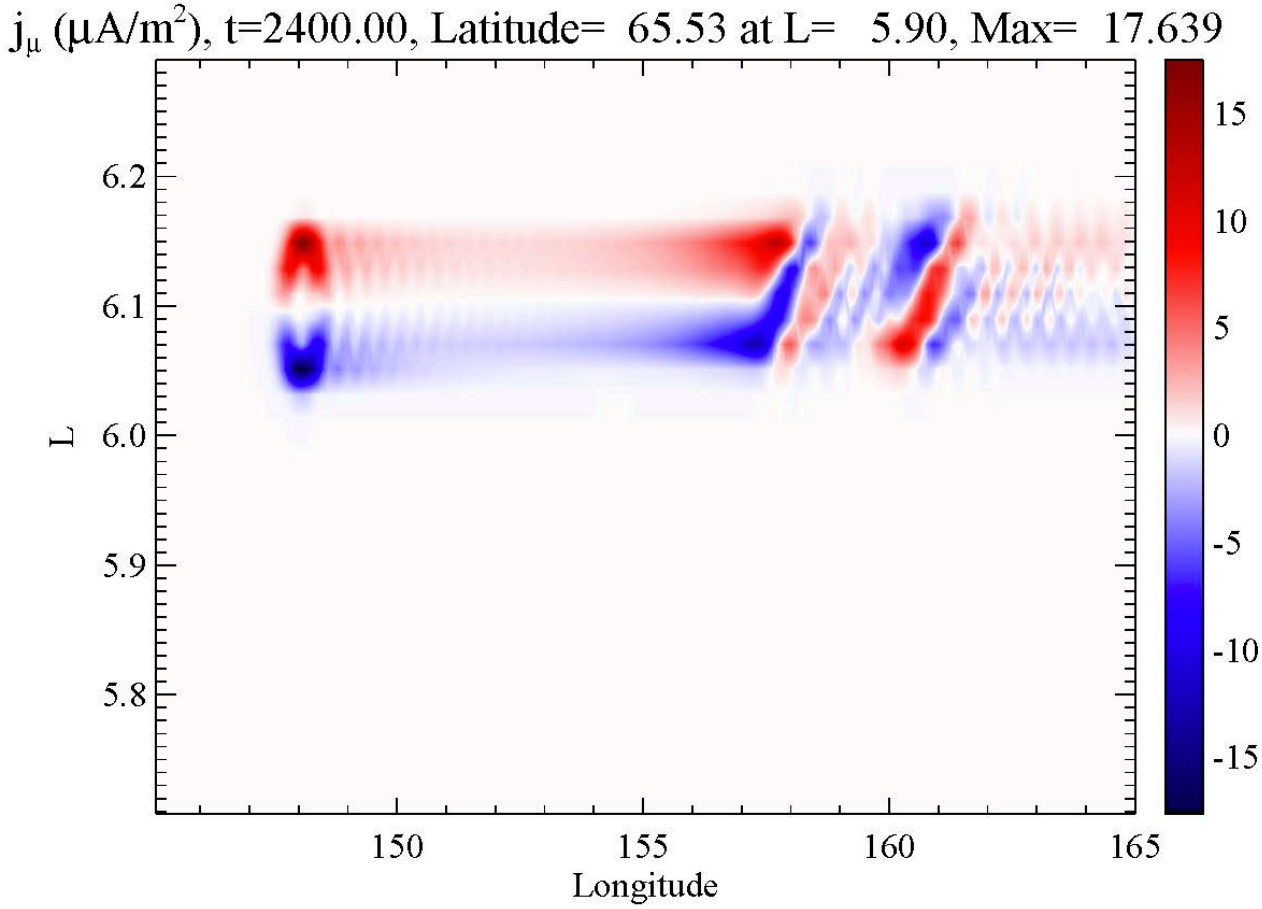

complicated pattern as in the Poynting flux plot. Figure 4b for the high-density case shows similar features, with the MAW and RAW currents farther apart, as in Figure 2.

The situation is modified when Io is near the boundary of the torus. Figures 5a (low-density case) and 5b (high-density case) show the Poynting flux in the region where Io is at its most northerly latitude. In this case, the main Alfvén wing arrives at the northern ionosphere before the waves arrive at the southern ionosphere since they spend less time in the plasma torus. In this case, the MAW and RAW in the northern hemisphere are farther apart (about 9° of longitude) while they are closer together (3° of longitude) in the southern hemisphere. In addition, the reflection from the northern torus boundary and the northern ionosphere are very close together since both of these waves must traverse nearly the entire plasma torus. The secondary waves between the ionosphere and torus are weaker in the north and stronger in the south, particularly between the MAW and RAW in that hemisphere. This pattern is reversed between the hemispheres when Io is near the southern boundary of the torus (not shown). The run shown

in Figure 5a is shown as an animation in Supporting Information S2.

The currents at the ionosphere also show these features. Figures 6a and 6b show the field-aligned current in the northern ionosphere for the two cases, while Figures 6c and 6d show the corresponding currents in the southern ionosphere. Note that positive (red) field-aligned currents in both hemispheres are northward along the field line, so upward current in the southern hemisphere is red. The strongest currents in both hemispheres are associated with the RAW and

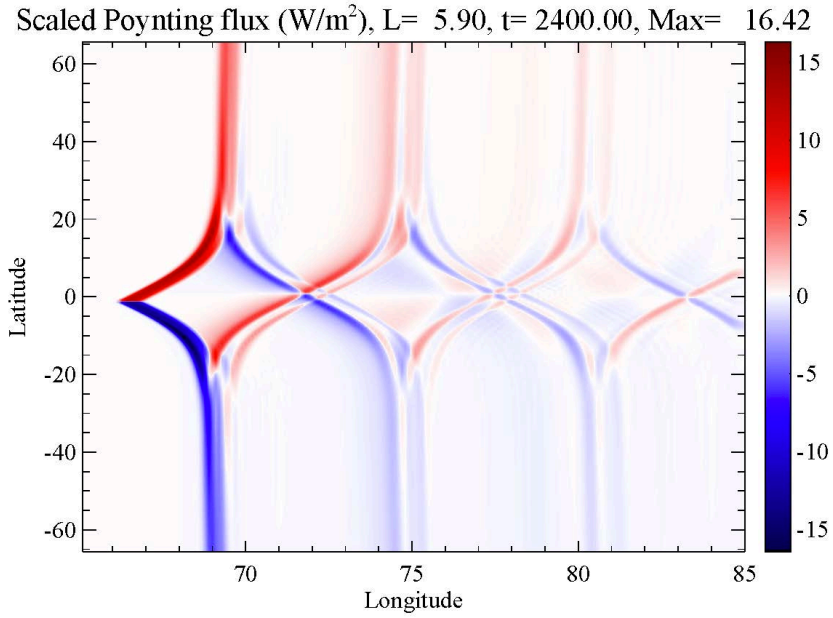

MAW; however, there are weaker currents associated with the secondary waves. The currents are somewhat weaker than when Io is near the equator, and they are weaker in the southern hemisphere than in the north. As in the previous runs, the U shape of the main spot is due to the changing cross section of Io and its ionosphere as it crosses field lines; this structure is maintained in the reflected waves. This pattern is more distinct in the northern hemisphere currents, suggesting that the pattern is washed out to some degree passing through the plasma torus. In the northern hemisphere, the current pattern is similar to the symmetric case with the upward field-aligned current occurring at the lower L-shells; however, in the southern hemisphere the MAW and RAW spots are closer together with significant currents between them.

4 Ionospheric conductance effects

The model includes a height-integrated conductance in Jupiter's ionosphere. The runs presented so far all considered a Pedersen conductance of 1 S. However, Gérard et al. (2020) have used data from the Ultraviolet Spectral Imager (UVS) on Juno to make estimates of the Pedersen conductance, showing that it can range from 0.1 S to about 10 S, consistent with results from ionospheric modeling

(Millward et al., 2002; Ray et al., 2014). We have done a series of runs to see the effect of the variation of the conductance at Jupiter, using the low-density model discussed above. Figure 7 shows the Poynting flux for runs in which Io is near the equator as in Figures 2a. Figure 7a shows the 0.1 S case, while Figure 7b gives the results for a Pedersen conductance of 10 S. In the low-conductance case, the ionosphere is closely matched to the Alfvén wave impedance and the wave is largely absorbed there. It can be seen that the reflection from the torus boundary is stronger than the reflection from the ionosphere. On the other hand, the reflection from the ionosphere in the 10 S case is very strong and does not lead to damping of the wave. In this case the secondary waves are enhanced compared to the lower conductance case.

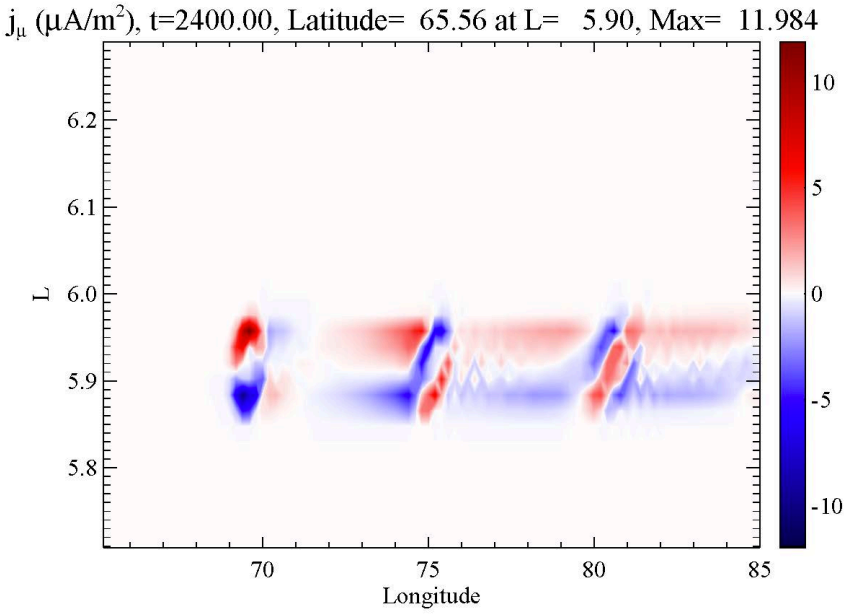

To quantify the amount of reflection in each case, we have decomposed the electric and magnetic fields into the so-called Elsässer variables (Elsässer, 1950), which for Alfvén waves can be written as , where the plus sign refers to waves propagating in the + direction (i.e., northward along the field line) and the minus sign to waves in the − direction. Evaluating these values at a latitude of 50° in the main Alfvén wing, we find that the reflection coefficients are 2.0%, 36.5% and 71.4% for the 0.1, 1.0 and 10.0 S cases, respectively. Mura et al. (2018) have shown that the tails can extend for over 100° in longitude around Jupiter. While these results favor a high Pedersen conductance, it is difficult to explain such extended tails even for the 10 S case.

The field-aligned currents at the ionosphere show similar characteristics. Figures 8a and 8b show the currents in the northern hemisphere for the runs shown in Figures 7a and 7b, respectively. A first point is that, unsurprisingly, the

currents are stronger for higher conductance. The low conductance case shows a near absence of current between the MAW and RAW spots, and by the second reflected spot, the currents are much weaker. On the other hand, in the high conductance case the currents remain strong between the MAW and RAW, although still weaker than the MAW spot. In this case, there are strong reflections at both the ionosphere and the torus boundary. Reflections from the low Alfvén speed torus and the high conductance ionosphere both lead to reduction in the electric field and enhancement in the field-aligned current, leading to stronger currents even though the Poynting flux is low in between the main spots. In the high conductance case, the upward and downward currents are seen to switch positions due to multiple reflections and phase mixing as the waves propagate. These simulations suggest that a strong and relatively continuous current structure would be associated with high ionospheric conductance. This effect is possibly related to the bifurcated footprint seen far down the Io tail by Mura et al. (2018) and Szalay et al. (2018).

5 Parallel Electric Fields: Current limitation

The models described above only included the effects of electron inertia on the formation of parallel electric fields. Inertial electric fields are favored when the perpendicular wavelength is comparable to the electron inertial length. In the low-density model, the lowest density is 0.1 cm^{-3}, corresponding to an inertial length of 17 km; Io's radius of 1820 km mapped to the ionosphere is about 140 km, much larger than the inertial length. Therefore, the inertial fields are small, with the parallel fields integrated along the field line being the order of 500 volts. However, the resulting field-aligned currents can be very large, 15-20 A/m^2 as can be seen in Figures 4 and 6. Kinetic modeling of the Io flux tube (Ray et al., 2009) indicates that such large currents cannot be supported without the formation of large potential drops along the field lines. Thus, the effect of these parallel potential drops should be taken into account.

One difficulty in including this type of potential drop in the present model is that the Ray et al. (2009) formulation relates the field-aligned current to the total potential drop on the field line, while the present model includes the parallel electric field at each point along the field line. However, we can model this effect by including a current-limiting term in the equations. The maximum current that can be carried by a Maxwellian distribution with no bulk acceleration is for the case of a totally empty loss cone, i.e., a half-Maxwellian distribution with only one sign of the parallel velocity. In this case, the effective drift velocity is , where the electron temperature is given in electron volts. Thus, the maximum current is $j_{max} = nev_d$, which is 3.39 A/m^2 for a density of 1 cm^{-3} and a temperature of 1 keV.

The parallel electric field can then be modeled by introducing the * term in the equation for the field-aligned current in equation . This term should be zero when the current is less than j_{max} and increase rapidly as the current increases above this value. For this model, we choose the form

The parameter * is set to zero for weaker currents. The constant $_0$ can be estimated from the linear form of the Knight (1973) relation, $j = K\Phi$, where . The effective parallel conductivity is then $= KL$, where L is the distance over which the parallel field is distributed. Then we can write

Where L is in Jovian radii and we have again taken $n = 1$ cm^{-3} and $T_e =$ 1keV. Thus, if we take this scale length to be about half a Jovian radius, we can conveniently set $_0 = 1$ s^{-1}.

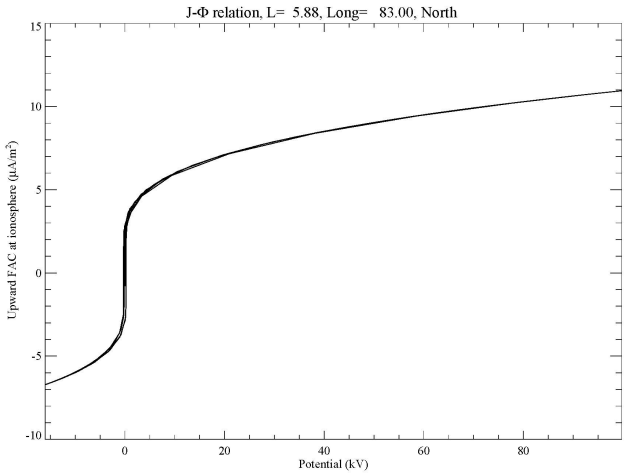

Figure 9 shows the resulting relationship between the parallel potential drop (more precisely, the integrated parallel electric field, since the field is not purely electrostatic) and the field-aligned current at the ionosphere with these parameters for a run that is otherwise the same as that shown in Figures 7b and 8b, which is the low-density case and a Pedersen conductance of 10 S at Jupiter. This figure shows the current-limiting effect of our model, with the currents being limited to about 10 A/m^2 leading to potentials up to 100 kV. These parameters are consistent with the kinetic results of Ray et al. (2009), indicating that our model is a reasonable approximation to these results.

Figure 10a shows the field-aligned current from this run. The current pattern is spread out somewhat from the corresponding run without the parallel electric field (Figure 8b). Strong parallel electric fields lead to a perpendicular component of the Poynting flux that broadens the magnetic perturbation. The amplitude of the magnetic perturbation fixes the total current that should flow in the flux tube, so that the current limitation requires the current to flow over a larger area. This leads to a splitting of the current pattern. In addition, the current is limited to about 10 A/m^2 compared to almost twice that in Figure 9b. Figure 10b shows the parallel potential. The color bar in this figure has been limited to 25 kV to bring out some of the weaker potentials (the actual potential in the main spot is about 100 kV as in Figure 9. Note that in contrast to the field-aligned current plot, the red colors indicate regions of upward parallel electric field.

These figures show that while the main spots are accompanied by strong parallel electric fields, the secondary reflections of the wave from the torus boundary are not. This is largely due to the current-limiting nature of the current-voltage relation. This raises the question of how these auroral features in this region, as seen in the JIRAM data, are generated. It is likely that effects not included in our model, such as the filamentation of the currents due to nonlinear effects or feedback from the ionosphere, are important.

6 Discussion

This work has presented initial results from a full-wave model of the propagation of Io-related Alfvén waves through the Jovian magnetosphere. While this is an improvement upon earlier models involving ray-tracing or simplified box geometries, it still neglects a number of features that can affect the structure and dynamics of the Io-generated aurora. Most importantly, the acceleration of the auroral particles themselves is not modeled. For example, the model does not take into account the presence of the transhemispheric electron beams, thought to be produced by electrons accelerated by Alfvén waves in the torus itself. Nevertheless, a number of features in the observations of the Io tail may be understood by the model results.

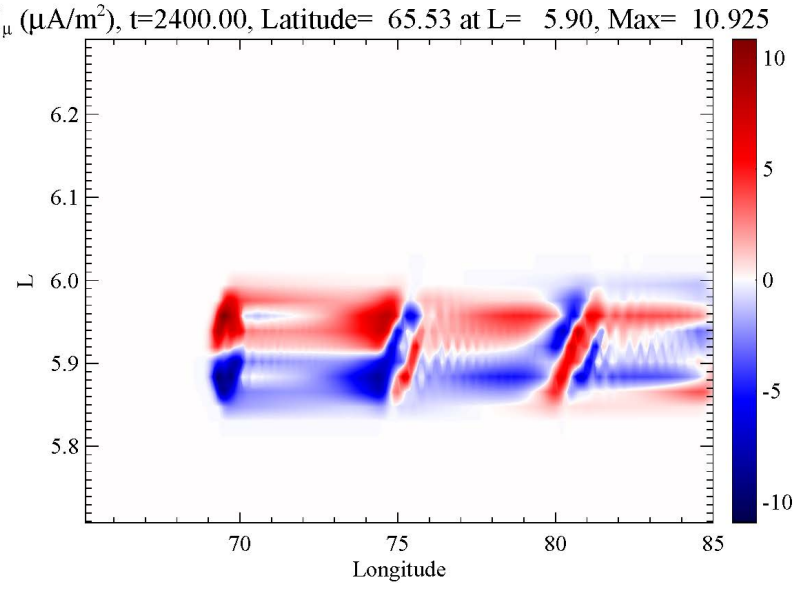

The overall structure of the main auroral spots is consistent with the expectations from ray-tracing models (e.g., Hinton et al., 2019). Our model indicates that the spacing of the main and reflected Alfvén wings is consistent with previous work and depends upon the density profile along the flux tube. Furthermore, the structure of the field-aligned currents produced by the model is consistent with the transverse displacement in secondary spots observed by JIRAM (Mura et al., 2018). The results suggest that this may be due to the generation of

field-aligned currents at the surface of Io and its ionosphere. In addition, the secondary structure in the currents is consistent with the reflection of Alfvén waves from the boundary of plasma torus, which can occur over time scales of about a minute. However, one puzzle in the results is that when the parallel electric fields due to current limitation are included, these secondary reflections do not produce significant potential drops.

The complicated structure after the passage of the RAW suggests that the waves are subject to phase mixing, particularly while passing through the dense plasma torus. This makes the current structure more complicated, especially after the passage of the reflected Alfvén wing. Recently, Schlegel and Saur (2022) considered the effect of different travel times on the alternating spots and concluded that this was only a minor effect. However, in our model, the difference in the passage time of an Alfvén wave from one ionosphere to another between L=5.90 and 5.95, a difference of about 1 Io radius, is 22.5 seconds in the low-density model and 30.6 seconds in high-density model, much larger than their assumed time of 3.7 seconds. In addition, the RAW spot occurs after the wave has traveled through the torus 1.5 times, so the difference is 50% larger. So it appears plausible that the travel time difference, i.e., phase mixing, can be an important effect down the tail from the main spot. This may be related to the bifurcated auroral tail sometimes seen downstream from main spot (Szalay et al., 2018; Mura et al., 2018).

In summary, this new model for the propagation of Alfvén waves generated by Io has revealed some interesting points and raised some questions about this interaction:

- The model confirms that reflections from the torus boundary are significant and give rise to the overall pattern of currents, indicating that the spacing of auroral emissions is dependent on the density along the flux tube. The transmission through the torus boundary is stronger in the high-density case since the density contrast is not as large, leading to higher currents at the ionosphere for this case.
- The Alfvén wave pattern depends strongly onthe position of Io within the plasma torus. The main and reflected Alfvén wings are farther apart and the magnitude of the currents is stronger in the northern hemisphere when Io is in this hemisphere.
- In addition to the main reflections, there are weaker secondary reflections of waves bouncing between Jupiter's ionosphere and the plasma torus. These may be responsible for the continued auroral emissions between the MAW and RAW spots. These secondary reflections appear to be particularly strong in the hemisphere opposite to the location of Io.
- The field-aligned currents due to the main Alfvén wing (MAW) have a characteristic U-shape due to the generation of field-

aligned currents at the Jupiter-facing and anti-Jupiter side of Io. The repetition of this shape due to the secondary reflections may be related to the structure of the auroral emissions as seen by JIRAM (Mura et al., 2018).

- The length of the footprint tail is a function of the conductance in Jupiter's ionosphere. A conductance of 0.1 S leads to strong dissipation of the wave on each bounce, while for a 10 S conductance the waves can persist for many bounces. However, the tails extending over 100° in longitude reported by Mura et al. (2018) may require more than the linear propagation of the Alfvén waves.
- The currents produced by Io are strong enough to lead to potential drops of up to 100 kV along the main Alfvén wing. However, the current limitation due to these potential drops keeps the currents in the secondary reflections limited, so that it is not clear from the present work how particles are accelerated by these reflected waves.
- At long distances along the tail, phase mixing and the presence of multiple reflected waves can complicate the structure of the currents. For high conductance in the ionosphere, the upward and downward currents can reverse with the upward currents appearing on the high latitude side of the footprint.

While this model shows some interesting features, there are still many unanswered questions. Although our model includes the electron inertial effect thought to be responsible for the electric field producing a broadband electron distribution, there does not seem to be significant electric fields produced by this effect. This may be due to the large size of Juno with respect to the electron inertial length. However, if the currents are strongly filamented, the importance of the electron inertial effect would be increased. Including the possibility of a turbulent cascade to smaller scales (Hess et al., 2010; Saur et al., 2002) or ionospheric feedback effects (Lysak, 1991; Lysak and Song, 2002; Moirano et al., 2021) would give a more complete understanding of the propagation of Io-generated Alfvén waves in Jupiter's magnetosphere.

Acknowledgments

This research has benefited from discussions with Jamey Szalay, Licia Ray, Alessandro Mura and Alessandro Moirano. This work has been supported by by NASA Grant 80NSSC20K1269 to the University of Minnesota. A.H.S. acknowledges support from NASA NFDAP grant 80NSSC21K1242. The work at the University of Colorado was supported as a part of NASA's Juno mission, supported by NASA through contract 699050X with the Southwest Research Institute.

Open Research Section

The codes used to simulate the propagation of Alfvén waves generated by the Io interaction with Jupiter's magnetosphere as well as the IDL software used to display the data and produce the figures in this manuscript have been deposited in the Data Repository for the University of Minnesota (DRUM) at https://conservancy.umn.edu/handel/11299/166578.

References

Acuña, M. H., Neubauer, F. M., & Ness, N. F. (1981). Standing Alfven wave current system at Io - Voyager 1 observations. *Journal of Geophysical Research, 86*(A10), 8513–8521. http://doi.org/10.1029/JA086iA10p08513

Bagenal, F. (1983). Alfven wave propagation in the Io plasma torus. *Journal of Geophysical Research, 88*(A4), 3013–3025. https://doi.org/10.1029/JA088iA04p03013

Bagenal, F. & Dols, V. (2020) The space environment of Io and Europa, *Journal of Geophysical Research: Space Physics, 125,* e2019JA027485. https://doi.org/10.1029/2019JA027485

Belcher, J. W., Goertz, C. K., Sullivan, J. D., & Acuna, M. H. (1981). Plasma observations of the Alfvén wave generated by Io. *Journal of Geophysical Research, 30,* 8508–8512. https://doi.org/10.1029/JA086iA10p08508

Bigg, E. K. (1964). Influence of the satellite Io on Jupiter's decametric emission. *Nature, 203*, 1008. https://doi.org/10.1038/2031008a0.

Bonfond, B. Grodent, D. Gérard, J.-C. Radioti, A. Dols, V. Delamere, P.A. & Clarke, J.T. (2009). The Io UV footprint: location, inter-spot distances and tail vertical extent. *J. Geophys. Res. 114,* 7224

Bonfond, B. Grodent, D. Gérard, J.-C. Radioti, A. Saur, J. Jacobsen, S. (2008). UV Io footprint leading spot: a key feature for understanding the UV Io footprint multiplicity? *Geophys. Res. Lett. 35*, 5107

Bonfond, B., Hess, S., Gérard, J.-C., Grodent, D., Radioti, A., Chantry, V., Saur, J., Jacobsen, S., & Clarke, J. T. (2013). Evolution of the Io footprint brightness I: Far-UV observations, *Planet. Space Sci., 88,* 64.

Chust, T., Roux, A., Kurth, W. S., Gurnett, D. A., Kivelson, M. G., & Khurana, K. K. (2005) Are Io's Alfvén wings filamented? Galileo observations, *Planet. Space Sci., 53,* 395.

Clarke, J. T., Ajello, J., Ballester, G., Jaffel, L. B., Connerney, J., Gérard, J.-C., Gladstone, G R., Grodent, D., Pryor, W., Trauger, J., & Waite, J. H. (2002). Ultraviolet auroral emissions from the magnetic footprints of Io, Ganymede, and Europa on Jupiter, *Nature, 415.* 997.

Clarke, J. T., Ballester, G. E., Trauger, J., Evans, R., Connerney, J. E. P., Stapelfeldt, K., et al. (1996). Far-ultraviolet imaging of Jupiter's aurora and the Io "footprint"'. *Science, 274*(5286), 404–409. https://doi.org/10.1126/science.274.5286.404

Connerney, J. E. P., Baron, R., Satch, T., & Owen T. (1993). Images of excited H_3^+ at the foot of the Io flux tube in Jupiter's Atmosphere, *Science, 262,* 1035.

Connerney, J. E. P., Kotsiaros, S.,Oliversen, R. J., Espley, J. R., Joergensen, J. L., Joergensen, P. S., et al. (2018). A new model of Jupiter's magnetic field from Juno's first nine orbits. *Geophysical Research Letters, 45,* 2590–2596. https://doi.org/10.1002/2018GL077312

Connerney, J. E. P., Timmins, S., Oliversen, R. J., Espley, J. R., Joergensen, J. L., Kotsiaros, S., et al. (2022). A new model of Jupiter's magnetic field at the completion of Juno's Prime Mission. Journal of Geophysical Research: Planets, 127, e2021JE007055. https://doi.org/10.1029/2021JE007055

Crary, F. J, & Bagenal, F. (1997). Coupling the plasma interaction at Io to Jupiter (1997). *Geophys. Res. Lett., 24,* 2135.

Dougherty L. P., Bodisch, K. M., & F. Bagenal (2017), Survey of Voyager plasma science ions at Jupiter: 2. Heavy ions, *J. Geophys. Res. Space Physics, 122,* doi:10.1002/2017JA024053.

Elsässer, W. M. (1950). The hydromagnetic equations, *Phys. Rev., 79,* 183.

Gérard, J.-C., Gkouvelis, L., Bonfond, B., Grodent, D., Gladstone, G. R., Hue, V., et al. (2020). Spatial distribution of the Pedersen conductance in the Jovian aurora from Juno-UVS spectral images. *Journal of Geophysical Research: Space Physics, 125*, e2020JA028142. https://doi.org/10.1029/2020JA028142

Goertz, C. (1980). Io's interaction with the plasma torus, *J. Geophys. Res., 85,* 2949-2956.

Gershman, D. J., Connerney, J. E. P., Kotsiaros, S., DiBraccio, G. A., Martos, Y. M., Viñas, A., et al. (2019). Alfvénic fluctuations associated with Jupiter's auroral emissions. *Geophysical Research Letters, 46.* https://doi.org/10.1029/2019GL082951

Goldreich, P. & Lynden-Bell, D. (1969). Io: a Jovian unipolar inductor, *Astrophys. J., 156,* 59.

Gurnett, D. A., & Goertz, C. K. (1981). Multiple Alfvén wave reflections excited by Io: Origin of the Jovian decametric arcs. Journal of Geophysical Research, 86(A2), 717–722. https://doi.org/10.1029/JA086iA02p00717

Hinton, P. C., Bagenal, F., & Bonfond, B. (2019). Alfvén wave propagation in the Io plasma torus. *Geophysical Research Letters, 46, 1*242–1249. https://doi.org/10.1029/2018GL081472

Jacobsen, S., Neubauer, F. M., Saur, J., & Schilling, N. (2007). Io's nonlinear MHD-wave field in the heterogeneous Jovian magnetosphere. *Geophysical Research Letters, 34,* L10202. https://doi.org/10.1029/2006GL029187

Lysak, R. L., & Song, Y. (2020). Field line resonances in Jupiter's magnetosphere, *Geophysical Research Letters, 47,* e2020GL089473, https://doi.org/10.1

029/2020GL089473

Lysak, R. L., Song, Y., Elliott, S., Kurth, W., Sulaiman, A. H., & Gershman, D. (2021). The Jovian ionospheric Alfvén resonator and auroral particle acceleration. *Journal of Geophysical Research: Space Physics, 126*, e2021JA029886. https://doi.org/10.1029/2021JA029886

Lysak, R. L., Song, Y., Sciffer, M. D., & Waters, C. L. (2015), Propagation of Pi2 pulsations in a dipole model of the magnetosphere*, J. Geophys. Res. Space Physics, 120,* doi:10.1002/2014JA020625.

Lysak, R. L., Song, Y., Waters, C. L., Sciffer, M. D., & Obana, Y. (2020). Numerical investigations of interhemispheric asymmetry due to ionospheric conductance. *Journal of Geophysical Research: Space Physics, 125,* e2020JA027866. https://doi.org/10.1029/2020JA027866

Mann, I. R., Wright, A. N., & Cally, P. S. (1995), Coupling of magnetospheric cavity modes to field line resonances: a study of resonant widths, *J. Geophys. Res., 100,* 19,441.

Mauk, B. H., Clark, G., Gladstone, G. R., Kotsiaros, S., Adriani, A., Allegrini, F., et al. (2020). Energetic particles and acceleration regions over Jupiter's polar cap and main aurora: A broad overview. Journal of Geophysical Research: Space Physics, 125, e2019JA027699. https://doi.org/10.1029/2019JA027699

Millward, G., Miller, S., Stallard, T., Aylward, A. D., & Achilleos, N. (2002). On the dynamics of the Jovian ionosphere and thermosphere. III. The modeling of auroral conductivity, Icarus, 160, 95-107. https://doi.org/10.1006/icar.2002.6951

Moirano, A., Mura, A., Adriani, A., Dols, V., Bonfond, B., Waite, J. H., et al. (2021). Morphology of the auroral tail of Io, Europa, and Ganymede from JIRAM L-band imager. *Journal of Geophysical Research: Space Physics, 126,* e2021JA029450. https://doi.org/10.1029/2021JA029450

Mura, A., Adriani, A., Altieri, F., Connerney, J. E. P., Bolton, S. J., Moriconi, M. L., et al. (2017). Infrared observations of Jovian aurora from Juno's first orbits: Main oval and satellite footprints: Jovian aurora IR observations from Juno. Geophysical Research Letters, 44(11), 5308–5316. https://doi.org/10.1002/2017GL072954

Mura, A., Adriani, A., Connerney, J. E. P., Bolton, S., Altieri, F., Bagenal, F., et al. (2018). Juno observations of spot structures and a split tail in Io-induced aurorae on Jupiter, *Science, 361,* 774-777. https://doi.org/10.1126/science.aat1450

Neubauer, F. M. (1980). Nonlinear standing Alfvén wave current system at Io: Theory, *J. Geophys. Res., 85,* 1171-1178.

Ray, L. C., Achilleos, N. A., M. F. Vogt, and J. N. Yates (2014), Local time variations in Jupiter's magnetosphere-ionosphere coupling system, J. Geophys.

Res. Space Physics, 119, 4740–4751, doi:10.1002/2014JA019941.

Ray, L. C., Su, Y.-J., Ergun, R. E., Delamere, P. A. & Bagenal, F. (2009), Current-voltage relation of a centrifugally confined plasma, *J. Geophys. Res., 114,* A04214, doi:10.1029/2008JA013969.

Saur, J. (2004). A model of Io's local electric field for a combined Alfvénic and unipolar inductor far-field coupling. *Journal of Geophysical Research, 109,* A01210. https://doi.org/10.1029/2002JA009354

Schlegel, S., & Saur, J. (2022). Alternating emission features in Io's footprint tail: magnetohydrodynamical simulations of possible causes. *Journal of Geophysical Research: Space Physics, 127,* e2021JA030243. https://doi.org/10.1029/2021JA030243

Sulaiman, A. H., Hospodarsky, G. B., Elliott, S. S., Kurth, W. S., Gurnett, D. A., Imai, M., et al. (2020). Wave-particle interactions associated with Io's auroral footprint: Evidence of Alfvén, ion cyclotron, and whistler modes. *Geophysical Research Letters, 47,* e2020GL088432. https://doi.org/10.1029/2020GL088432

Szalay, J. R., Bagenal, F., Allegrini, F., Bonfond, B., Clark, G., Connerney, J. E. P., et al. (2020). Proton acceleration by Io's Alfvénic interaction. *Journal of Geophysical Research: Space Physics, 125*, e2019JA027314. https://doi.org/10.1029/2019JA027314

Szalay, J. R., Bonfond, B., Allegrini, F., Bagenal, F., Bolton, S., Clark, G.. et al. (2018), In situ observations connected to the Io footprint tail aurora, *J. Geophys. Res.: Planets, 123,* 3061, doi: https://doi.org/10.1029/2018JE005752

Takahashi, K., Lysak, R., & Vellante, M. (2022). Statistical analysis of Pi2 pulsations observed by Van Allen Probes. *Journal of Geophysical Research: Space Physics, 127,* e2022JA030674. https://doi.org/10.1029/2022JA030674

Takahashi, K., Lysak, R. L., Vellante, M., Kletzing, C. A., Hartinger, M. D., & Smith, C. W. (2018), Observation and numerical simulation of cavity mode oscillations excited by an interplanetary shock, *J. Geophys. Res. Space Physics, 123*, 1969, doi: 10.1002/2017JA024639.

Open Research

AGU requires an Availability Statement for the underlying data needed to understand, evaluate, and build upon the reported research at the time of peer review and publication. Additionally, authors should include an Availability Statement for the software that has a significant impact on the research. Details and templates are in the Availability Statement section of the Data & Software for Authors Guidance. For physical samples, use the IGSN persistent identifier, see the International Geo Sample Numbers section.

References

References in supporting information must also be included in the reference list of the main paper, or in a designated section in the main paper so that they will be discovered, linked, and indexed. A separate list in the supporting information is not necessary. References are not included in word counts for excess length fees.

In the References section, cite the data/software described in the Availability Statement (this includes primary and processed data used for your research). For details on data/software citation as well as examples, see the Data & Software Citation section of the Data & Software for Authors guidance.

All references must be available to readers at the time of publication; there should be no "unpublished", in preparation, under review, or "in press" references. Please write the respective journal with any questions.

An example of a reference:

Deng, A., & Stauffer, D. R. (2006), On improving 4-km mesoscale model simulations. *Journal of Applied Meteorology and Climatology*, *45*(3), 361–381. doi:10.1175/JAM2341.1

More information on reference formatting with examples can be found in our Brief Guide to AGU Style.

Figure 1. The figure caption should begin with an overall descriptive statement of the figure followed by additional text. They should be immediately after each figure. Figure parts are indicated with lowercase letters (a, b, c...). For initial submission, please place both the figures and captions in the text near where they are cited rather than at the end of the file (not both). At revision, captions can be placed in-text or at the end of the file, and figures should be uploaded separately. Each figure should be one complete, cohesive file (please do not upload sub-figures or figure parts in separate files). Data that supports the figure must be preserved in a repository, included in the Open Research section, and cited in the References. Include detailed information on how to recreate the figure in support of transparency (e.g., Python, R library).

Table 1. Start this caption with a short description of your table. Format tables using the Word Table commands and structures. Additional information on table formatting can be found in our Style Guide, Table Formatting. Do not create tables using spaces or tab characters. Large tables should not be included in the main text of the paper, but instead preserved as a .csv file in a repository. All data displayed in tables must be preserved in a repository, included in the Open Research section, and cited in the References.

Figure 1. The figure caption should begin with an overall descriptive statement of the figure followed by additional text. They should be immediately after each figure. Figure parts are indicated with lower-case letters (**a, b, c...**). For initial submission, please place both the figures and captions in the text near where they are cited rather than at the end of the file (not both). At revision, captions can be placed in-text or at the end of the file, and figures should be uploaded separately. Each figure should be one complete, cohesive file (please do not upload sub-figures or figure parts in separate files).

Table 1. Start this caption with a short description of your table. Format tables using the Word Table commands and structures. Additional information on table formatting can be found in our Style Guide, Table Formatting. Do not create tables using spaces or tabs characters. Large tables presenting rich data should be presented as separate excel or .csv files, not as part of the main text.